



Wave forces on vertical caissons with retreated wall: A first experimental insight

Alessandro Romano ^{a,b,*}, Giorgio Bellotti ^a

^a Roma Tre University, Engineering Department, Rome 00146, Italy

^b IH Cantabria - Instituto de Hidráulica Ambiental de la Universidad de Cantabria, Calle Isabel Torres 15, Santander 39011, Spain

ARTICLE INFO

Keywords:

Vertical breakwaters
Retreated wall
Wave-induced forces
Physical model tests
Water waves

ABSTRACT

This paper presents a physical model study of wave induced forces on a composite vertical breakwater, where the crown wave wall is retreated with respect to the front face of the caisson. Four different configurations (one flushed wall and three retreated wall configurations) have been tested under regular wave conditions, aiming at providing a first experimental insight on the increase/reduction of the wave loads acting on the structure. The analysis of the experimental results allows to describe the basic phenomena involved and to identify the physical/geometrical drivers, which are expected to play a role on the force increase/reduction factor. Thus, detailed processing of both forces/moments (synchronous analysis) and pressures (asynchronous analysis) on the whole structure, the wall and the caisson trunk, together with the analysis of reflection coefficients as a function of the wall position, are presented and discussed in the paper. The experimental evidences suggest that, at least for the four configurations tested, the global forces acting on the caisson vary significantly depending on the wall position, resulting in a reduction between 5% and 31% for high energy sea states. A similar behavior is found considering the global moments. Furthermore, the synchronous analysis of the forces highlighted that the physical/geometrical drivers, identified in the present study, can have both a concordant and antithetical action among them, then resulting in increasing or decreasing, respectively, forces acting on the structure, if compared with the flushed wall configuration.

1. Introduction

Composite vertical breakwaters are monolithic structures often used to protect harbor basins, especially in relatively deep water conditions. Currently, design criteria of composite vertical breakwaters are mainly based on the Goda's formulae (Goda, 2010), including impulsive breaking conditions proposed by Takahashi (1996). More recently, Oumeraci et al. (2001) has provided guidelines for the design of composite vertical breakwaters and seawalls under breaking and non-breaking conditions within the framework of PROVERBS (PRObabilistic design tools for VERTical Breakwaters); these guidelines also include methods to estimate wave impact magnitude and duration on vertical breakwaters (Martinelli and Lamberti, 2011). Many research works addressed the study of wave loads induced by breaking waves on vertical walls placed in shallow water conditions (e.g., Cooker and Peregrine, 1990; Bullock et al., 2007; Bredmose et al., 2009; Cuomo et al., 2010a,b; Bredmose et al., 2015). On the contrary, less research is available on the engineering optimization of composite vertical breakwaters in relatively deep water conditions.

In fact, due to the significant size of this kind of structures, their engineering optimization, i.e., reduction of the forces acting on them

and/or improving their hydraulics performance, by reducing the reflection coefficient and/or the wave overtopping without varying significantly the geometric dimension of the structure themselves, may result in a significant economic saving. As far as wave overtopping reduction is concerned, there exist several viable technical solutions, like for instance the use of an overhang or a curved parapet. These solutions are extremely effective in reducing wave overtopping, but, at the same time, introduce the possibility of occurrence of impulsive loads for both breaking and non-breaking wave conditions (Kortenhaus et al., 2002, 2004; Pearson et al., 2005; Kisacik et al., 2012, 2014; Stagonas et al., 2014; Martinelli et al., 2018; Castellino et al., 2018; de Almeida and Hofland, 2020; Ravindar et al., 2021), which might be not considered by the standard design criteria (Castellino et al., 2021).

Another widespread technical solution often used for both reducing wave loads on the structure and limiting wave overtopping consists in placing the crown wall on a retreated position with respect to the seaside edge of the caisson trunk. An example of this solution is represented in Figure 7.1 of the EurOtop manual (EurOtop, 2007), depicting the Civitavecchia vertical breakwater (Italy). This solution is

* Corresponding author at: Roma Tre University, Engineering Department, Rome 00146, Italy.

E-mail address: alessandro.romano@uniroma3.it (A. Romano).

supposed to favor, due to geometric reasons, a time shifting between the dynamic loads acting on the caisson trunk and the wave wall. At the same time, modifying the pulsating nature of the wave–structure interaction hydrodynamics, it introduces extra turbulent dissipations that would favor the wave overtopping reduction. Nevertheless, also in this case, the nature of wave loads, at least of those acting on the retreated wall, could change, eventually giving rise to impulsive wave loads.

It is worth to highlight that there no exist specific design criteria, nor guidelines, to consider the effects, in terms of acting forces on the structure, of retreated walls on composite vertical breakwaters. Indeed, studies that investigate forces and pressures on retreated walls placed on tops of smooth dikes and rubble mound breakwaters are available (e.g., Martin et al., 1999; van Gent, 2003; De Rouck et al., 2012; Chen et al., 2015; Van Doorslaer et al., 2017; Molines et al., 2019; De Finis et al., 2020; Cao et al., 2021; Chen et al., 2021), but there is a lack of studies on retreated walls placed on top of composite vertical breakwaters placed in relatively deep water conditions. Specifically, to the best knowledge of the Authors, guidelines are not available to estimate the global force increase/reduction (if any), as well as the eventual nature change of the loads acting on the wall (i.e., impulsive loads), induced by a retreated crown wall placed on the top of a composite vertical breakwater.

In this paper, a series of physical model experiments aiming at investigating the wave forces acting on an ideal composite vertical breakwater as a function of the crown wave wall retreat position has been carried out. The aim of this campaign is to provide a first experimental insight on the increase/reduction of the wave loads acting on the whole structure, the wall and the caisson trunk. Thus, four different retreated wall configurations (one flushed wall and three retreated wall configurations) have been tested in a 2DV wave flume under regular wave conditions, by varying both wave height and wave period. Furthermore, the experimental campaign aims at investigating the basic physical phenomena involved and to identify the physical/geometrical drivers, which are expected to play a role on the force increase/reduction factor. Moreover, the analysis of the reflection coefficient as a function of the wall position has been carried out. Finally, the research aims to present preliminary experimental evidences that will be used as base to provide in the future, with more analysis and further investigation (both physical and numerical modeling) also considering random sea waves, design guidelines or recommendations for this technical solution.

The paper is structured as follows. After this introduction, the description of the experimental setup, together with the model structure and the wave conditions, is provided. Then, a detailed description and discussion of the experimental results, together with the limitations of the present study, is given. Finally, conclusions and ongoing research close the paper.

2. Experimental setup

2.1. Wave flume

The experiments have been carried out at the hydraulics laboratory of the Engineering Department of Roma Tre University (Rome, Italy). The facility is equipped with a wave flume which is 20.0 m long, 0.605 m wide and 1.0 m high. The side walls of the flume are made of glass and steel. The flume is equipped with a piston-type wave maker (maximum stroke equal to 1.35 m) which is able to generate both regular and irregular waves. The wave generation system is controlled by the state-of-the-art software AWASYS 7 (Aalborg University, 2018), including an Active Wave Absorption System (Andersen et al., 2016, 2018). The flume is equipped with seven resistive wave gauges (VTI Resistive Wave Gauge Modules installed in a WG-8CH rack) to measure the free surface elevation; five wave gauges, used for the reflection analysis, are located along the flume. The two remaining wave gauges

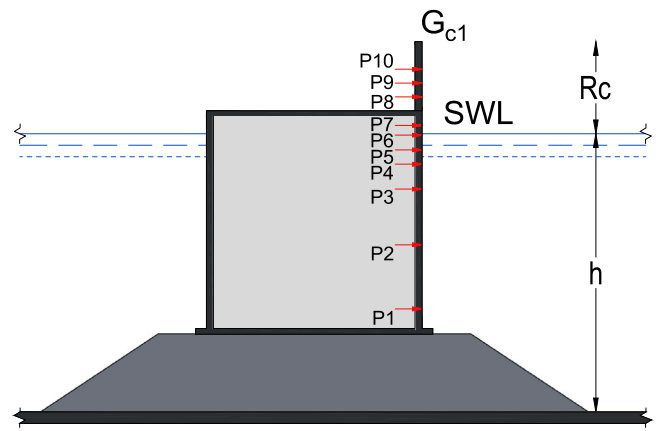


Fig. 1. Sketch of the vertical composite breakwater for the flushed wall configuration ($G_{c1} = 0.00$ m), and position of the pressure sensors on the caisson trunk (P_{1-7}) and wall (P_{8-10}).

are placed on the wave paddle and are used for the active wave absorption. The acquisition frequency of the wave probes is 50 Hz. The wave gauges are calibrated at least twice daily, to account for possible differences through the day in the laboratory environment.

2.2. Model structure: the composite vertical breakwater

The structure used during the experiments is a small-scale reproduction of an ideal composite vertical breakwater. The structure is made of marine plywood (thickness 0.015 m), to guarantee the stiffness of the structure, and is placed on top of a rubble mound foundation with a total height of $h_b = 0.17$ m, to resemble a real-case configuration of this kind of structures (see Fig. 1). The vertical breakwater is structurally divided into two parts, namely the trunk and the wall. The height of the caisson trunk is $h_t = 0.485$ m, while the height of the crown wall is $h_w = 0.15$ m. The wall is supported by a series of brackets, which have two main functions: I) to increase the stiffness of the wall itself; II) to fix, by using screws, the wall on the crown of the caisson. Thus, this fixing system allows to vary the position of the wall obtaining different retreated wall configurations. It is worth noticing that the physical model does not aim at reproducing a specific existing structure; on the contrary it has been designed aiming at being as general as possible, or, in other words to be representative, in a Froude similarity, of a wide range of vertical breakwater configurations built in relatively high water depths. Nevertheless, if a reference is needed, it could roughly resemble the caisson built to lengthen the main breakwater of the Civitavecchia harbor (Central Italy, Tyrrhenian Sea) configuration in a Froude law scale of 1:50.

To measure the loads applied by the waves on the structure, 10 pressure transducers (P_i , $i = 1, 2, \dots, 10$; TRAFAG Submersible Pressure Transmitter NAL 8838, pressure range 0.1–25.0 bar) have been installed on the seaside face of the vertical structure. Seven are placed on the caisson trunk (P_{1-7}), while three on the wall (P_{8-10} , see Fig. 1). The mutual distance between the pressure transducers is not constant (range of 0.025–0.11 m). On the wall and in proximity of the mean water level, where higher resolution is desirable, more sensors have been placed. The acquisition frequency of the pressure sensors is 7000 Hz, to allow the measurements of eventual impulsive loads.

As previously stated, the aim of these experiments lies in investigating the influence of the wave wall position, in terms of forces acting on the whole caisson on the wall itself and on the caisson trunk. Therefore, four geometric configurations have been reproduced. Each of them is characterized by a different value of the geometric structural parameter G_c , defined as the distance between the toe of the crown wave wall and the seaside edge of the caisson trunk crown. Consequently, if the

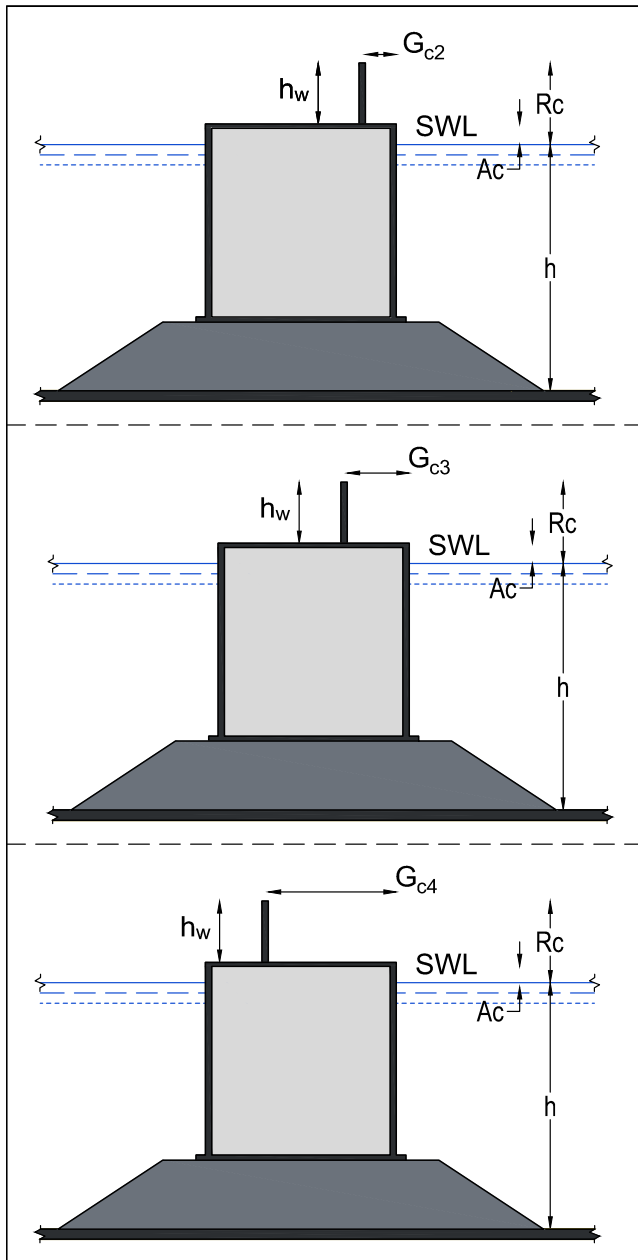


Fig. 2. Sketch of the three retreated wall configurations tested during the experiments and geometrical parameters of interest. Upper, middle and lower panels refer to the retreated wall configurations $G_{c2} = 0.075$ m, $G_{c3} = 0.15$ m, and $G_{c4} = 0.31$ m, respectively.

wall is aligned with the edge of the caisson trunk, then the wall is referred so as aligned or flushed wall ($G_c = 0.00$ m); otherwise it is referred as a retreated wall. With this in mind, the four configurations considered for the experiments are characterized by different values of G_c , namely: $G_{c1} = 0.00$ m (flushed wall, see Fig. 1), $G_{c2} = 0.075$ m (“small” wall retreat), $G_{c3} = 0.15$ m (“intermediate” wall retreat) and $G_{c4} = 0.31$ m (“large” wall retreat). Fig. 2 reports the three retreated wall configurations used during the experiments.

2.3. Wave conditions

In order to investigate the influence of the wall position on the loading conditions and to enucleate the basic physical phenomena

involved, only regular waves have been reproduced during the experiments. Thus, 19 regular wave conditions have been tested for each wall configuration, providing a total number of 76 experiments. Both the wave height H (spanning in the range $0.08 \leq H \leq 0.16$ m) and the wave period T ($T = 1.0, 1.1, 1.2, 1.5$ s) have been varied, aiming at providing a wide range of hydrodynamic conditions. The water depth has been kept constant during the experiments ($h = 0.625$ m). The duration of each test is approximately 120 s in order to obtain a wave time series long enough (i.e., several dozens of waves) to get stationary conditions acting on the structure.

3. Results and discussion

This section reports the analysis of the experimental results. Firstly, the wave reflection analysis, and the related discussion on the reflection coefficients, is presented. Secondly, an in-depth analysis of forces, moments and pressures acting on the structure is provided. The analysis of the wave loads aims at providing a clear description of the physical process at hand and, at the same time, to make the first step in the development of design guidelines/recommendations based on the experimental evidences. To this end, the analysis has been divided into four parts: I) description of the analysis procedure for the pressure time series; II) synchronous analysis of the forces and moments; III) asynchronous analysis of the pressures; IV) analysis of the force reduction/increase factor as a function of the wall position.

3.1. Wave reflection analysis

The wave reflection analysis has been carried out, for each test, to separate the incident (H_i) and reflected wave components by using the nonlinear method proposed by Andersen et al. (2017), to estimate the reflection coefficient of the structure. Thus, from now on, the wave height H , is intended to be the incident wave height H_i . Note that the reflection analysis, and consequently all the following analysis of forces and pressures, has been carried out in the time window 100–120 s, in which stationary conditions acting on the structure are guaranteed for each test.

Fig. 3 reports the reflection coefficient as a function of wave height and wave period ($T_1 = 1.0$ s, upper left panel; $T_2 = 1.1$ s, upper right panel; $T_3 = 1.2$ s, lower left panel; $T_4 = 1.5$ s, lower right panel). In the figure, full black dots refer to the flushed wall configuration ($G_{c1} = 0.00$ m), while full gray, red, and blue dots refer to G_{c2} , G_{c3} , and G_{c4} , respectively. Note that this color code is used throughout the whole manuscript.

Fig. 3 indicates that the reflection coefficient for flushed wall configuration (G_{c1}) ranges, as expected, between 0.82 and 0.98, showing a global pattern which is slightly decreasing for increasing wave height and wave period. This is coherent with the fact that, in general, the larger the wave height, the larger is the dissipation that occurs due to the wave interaction with the wall, with the basement and along the lateral sides of the flume. As far as retreated wall configurations are concerned, smaller values of the reflection coefficient are obtained, in the ranges 0.71–0.89, 0.71–0.87, and 0.66–0.87 for G_{c2} , G_{c3} , and G_{c4} , respectively. Again, also for retreated wall configurations, the reflection coefficient exhibits a global pattern which is slightly decreasing for increasing wave height and wave period.

It is interesting to note that for small values of the wall retreat (G_{c2}) the percentage reduction of the reflection coefficient is globally small (around 10% for the less energetic sea states), absent in some cases (for the high energetic sea states), while for large values of the wall retreat (G_{c3} and G_{c4}) the relative reduction of the reflection coefficient is larger, reaching a maximum value of 19% for G_{c4} (for the high energetic sea states).

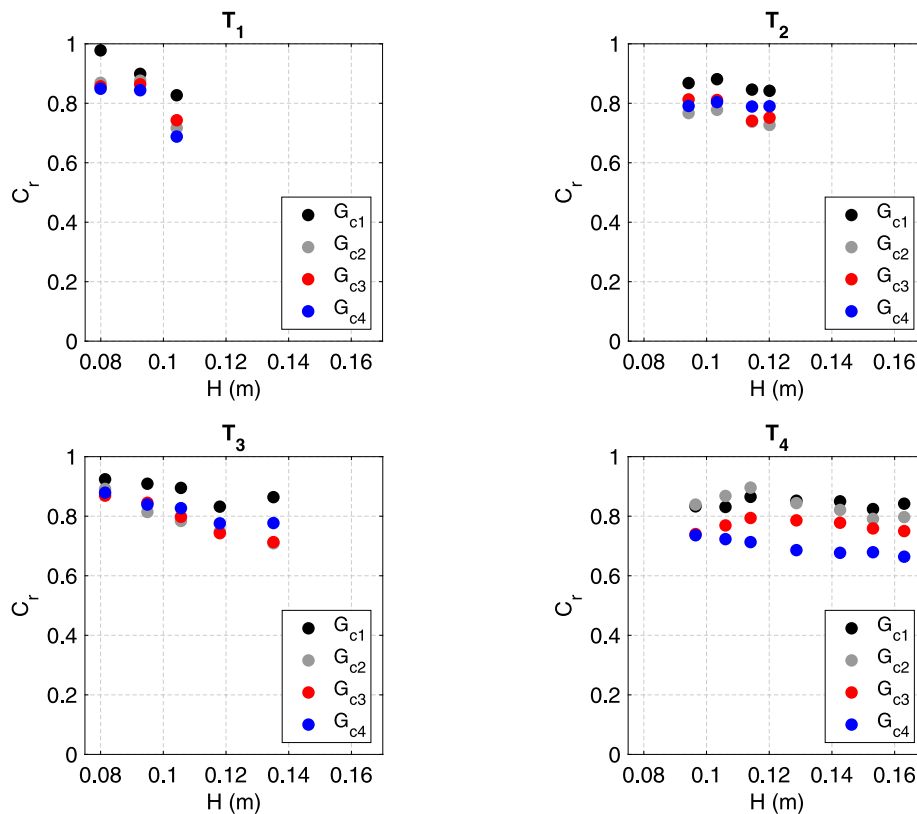


Fig. 3. Reflection coefficient as a function of wave height and wave period ($T_1 = 1.0$ s, upper left panel; $T_2 = 1.1$ s, upper right panel; $T_3 = 1.2$ s, lower left panel; $T_4 = 1.5$ s, lower right panel). Note: black dots refer to the flushed wall configuration ($G_{c1} = 0.00$ m), while gray, red, and blue dots refer to G_{c2} , G_{c3} , and G_{c4} , respectively.

3.2. Analysis procedure for the pressure time series

In this section the analysis procedure for the pressure time series is briefly described. Fig. 4 reports an example of the pressure signals measured at the ten pressure transducers ($P_1 - P_{10}$) for the flushed wall configuration (G_{c1}) in the time window 100–110 s under the wave condition $H = 0.16$ m, $T = 1.5$ s. Note that in the figure and throughout the rest of the paper, pressures have been converted to equivalent meters of water column. Fig. 4 shows the pulsating nature of the pressure induced by regular waves on the flushed wall configuration; this is a typical behavior for these kind of structures, especially if placed in relatively deep water conditions. In fact, at every time instant the pressure signals over the entire structure (trunk and wall) are perfectly in phase. Some of the pressure sensors become wet only for the wave crests.

Then, an example of the pressure signals measured for a retreated wall configuration (G_{c3}), under the same wave conditions, is reported in Fig. 5. Here a different wave–structure interaction mechanism occurs. The first significant difference lies in the fact that there is a clear distinction between the pressure signals acting on the trunk and those acting on the wall. In fact, the pressure signals measured at the trunk (P_{1-7}) still maintain a pulsating nature (although less regular), while those measured on the retreated wall (P_{8-10}) exhibit an impulsive-like impact (i.e., church-roof-like) nature. The shape of the pressure signals measured on the caisson trunk is less regular and slightly asymmetric than that observed on the flushed wall configuration (P_{1-4}). These irregular fluctuations of the pressure, are likely due to the backwash jets that flows down from the promenade. These jets, impacting into the water, increase the turbulent dissipation in front of the caisson trunk causing pressure fluctuations which are evident especially at the pressure sensors close to the still water level position (P_{5-7}). Finally, as expected, pressure peaks on caisson trunk and wall seem to be not in

phase in the retreated wall configuration. All these aspects are analyzed in details in the following sections.

Thus, for each experiment the pressure signals, measured by the ten pressure transducers, have been analyzed in the time window 100–120 s (i.e., the same used for the reflection analysis) after a preliminary visual quality check of the signals. The pressure time series have been used as input for both the synchronous analysis of the forces and the asynchronous analysis of the pressures (i.e., pressure diagrams acting on the structure).

As far as the synchronous analysis of the forces and moments is concerned, for each experiment the pressure signals have been integrated, considering for each sensor its area of influence, to obtain the horizontal force time series acting on the structure, and its distance from the considered pivot to the application point of the force, to obtain the moment time series acting on the structure. No filtering has been used. Moreover, the resulting force time series has been processed by considering separately the global force $F_G(t)$ (acting on the whole structure), the force acting on the wall $F_W(t)$ and the force acting on the caisson trunk $F_T(t)$ signals. Once the force signals have been obtained, a peaks over threshold (POT) analysis has been carried out to identify the force peaks within the above mentioned time window. Thus, for each experiment, and for each considered force signal ($F_G(t)$, $F_W(t)$ and $F_T(t)$), a series of force peak values is obtained. Since regular waves have been used, average values of these peaks over the time window (hereinafter F_G , F_W and F_T , respectively) are considered in the following analysis and discussion (see Section 3.3). Similarly to what done for the forces time series, the moments time series have been processed by considering separately the global moment $M_G(t)$ (acting on the whole structure, considering the pivot on the landside toe of the caisson), the moment acting on the wall $M_W(t)$ (considering the pivot on the landside toe of the wall) and the moment acting on the caisson trunk $M_T(t)$ (considering the pivot on the landside toe of the caisson) signals. Therefore, a POT analysis has been applied

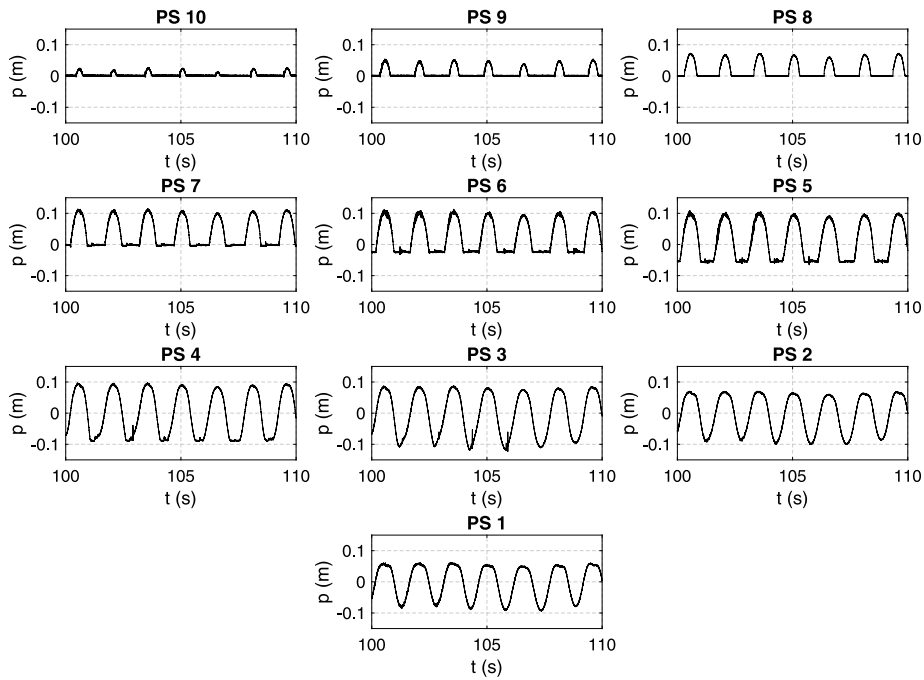


Fig. 4. Example of the pressure time series measured at the ten pressure transducers for the flushed wall configuration (G_{c1} , $H = 0.163$ m, $T = 1.5$ s).

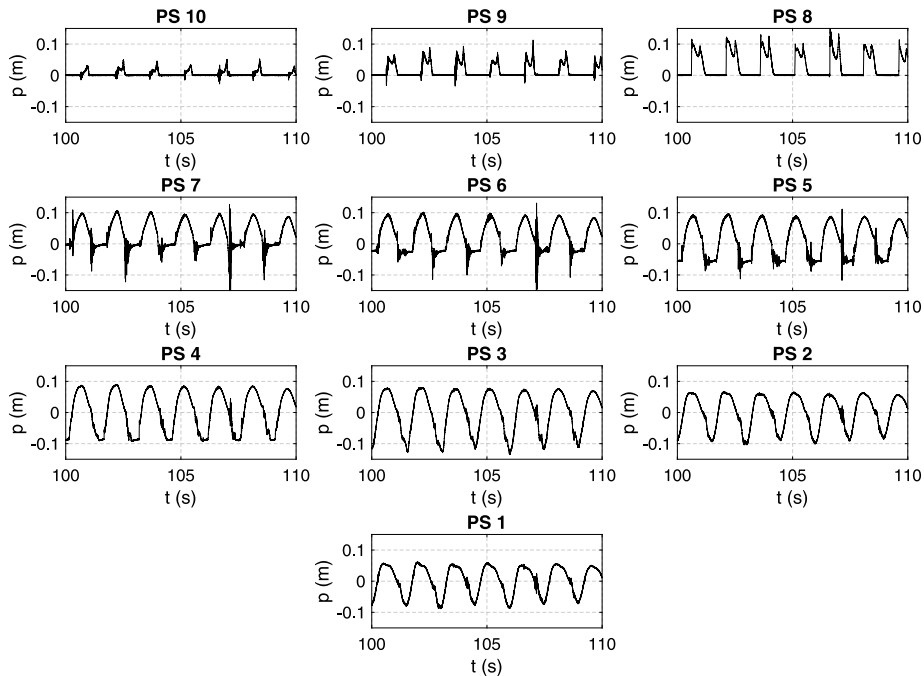


Fig. 5. Example of the pressure time series measured at the ten pressure transducers for a retreat wall configuration (G_{c3} , $H = 0.163$ m, $T = 1.5$ s).

to the moment signals ($M_G(t)$, $M_W(t)$ and $M_T(t)$) and the average values of the moment peaks over the time window (hereinafter M_G , M_W and M_T , respectively) are considered in the following analysis and discussion (see Section 3.3).

As far as the asynchronous analysis of the pressures is concerned, for each experiment each pressure time series has been processed by using the POT method, applied in the same time window already used for both the wave reflection analysis and the synchronous analysis of the forces, in order to obtain the pressure peaks at the z coordinate of each pressure transducer. Similarly to what done for the forces average values of these pressure peaks over the time window are considered in the following analysis and discussion (see Section 3.4).

3.3. Forces and moments: synchronous analysis

Synchronous analysis of the forces and moments are presented in Figs. 6 and 7. These figures are divided into twelve panels, distributed in four rows and three columns. Each row is referring to a different wave period (first, second, third, and fourth rows refer to T_1 , T_2 , T_3 , and T_4 , respectively), while each column refers to a different force or moment component acting on the structure (in Fig. 6 first, second, and third columns refer to the global F_G , wall F_W and trunk F_T forces, respectively; in Fig. 7 first, second, and third columns refer to the global M_G , wall M_W and trunk M_T moment, respectively).

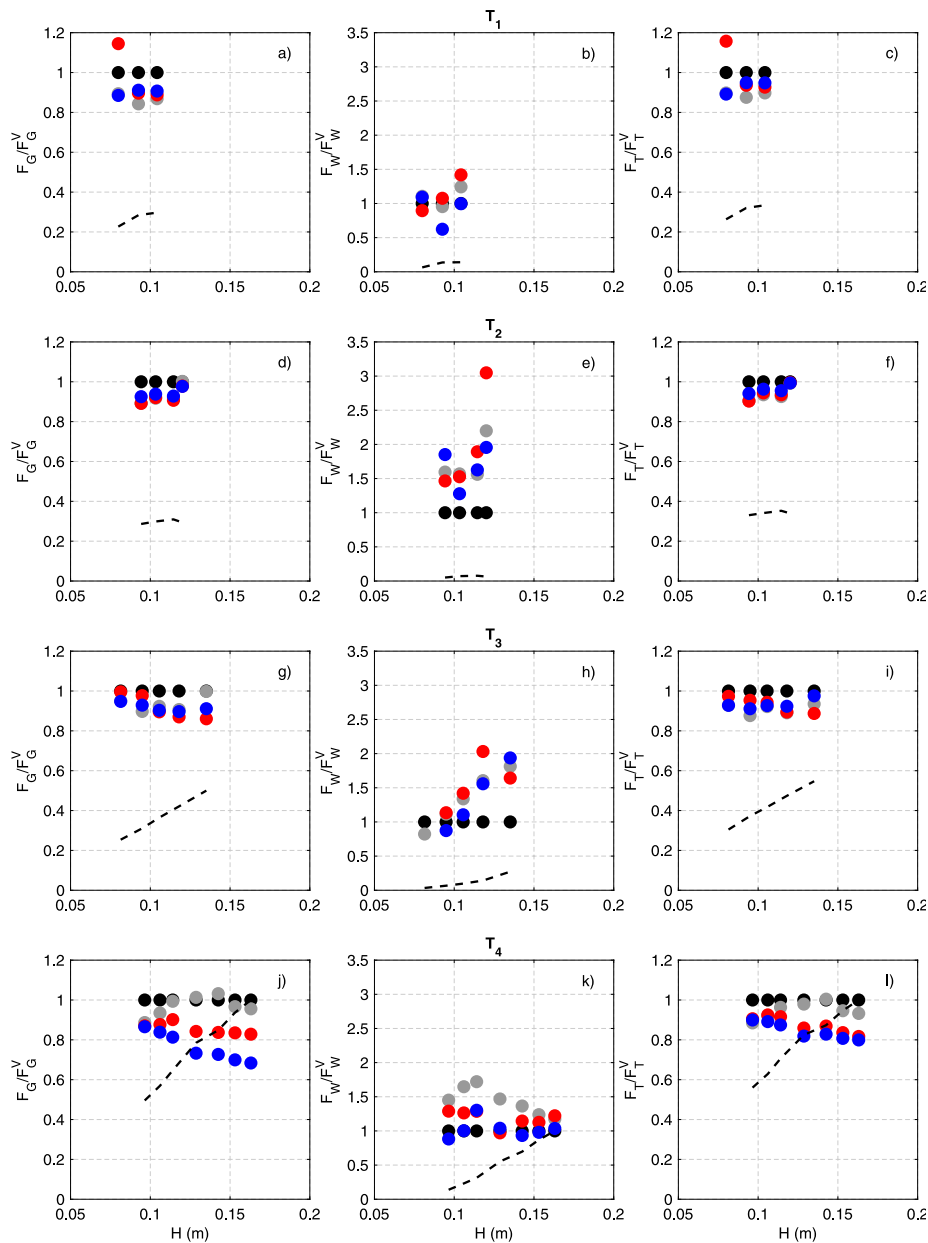


Fig. 6. Dimensionless global F_G/F_G^V , wall F_W/F_W^V , and trunk F_T/F_T^V forces as a function of the wave height for the four wall configurations. Note: each row refers to a different wave period (first, second, third, and fourth rows refer to T_1 , T_2 , T_3 , and T_4 , respectively), while each column refers to a different force component acting on the structure (first, second, and third columns refer to the global, wall and trunk forces, respectively). Full black, gray, red, and blue dots refer to G_{c1} (flushed wall), G_{c2} , G_{c3} , and G_{c4} , respectively. Black dashed lines represent $F_G^V/\max(F_G^V)$ (first column), $F_W^V/\max(F_W^V)$ (second column), $F_T^V/\max(F_T^V)$ (third column).

Note that all the data reported in Figs. 6 and 7 are dimensionless and plotted as a function of the wave height H . Specifically, the forces, related to each wall configuration, have been divided by F_G^V , F_W^V , F_T^V , which are the average global, wall and trunk forces, respectively, obtained for the flushed wall configuration (G_{c1}) in the considered test. Note that the apex $(\cdot)^V$, standing for “vertical”, is used from now on throughout the whole manuscript to identify quantities related to the flushed wall configuration. Similarly, the moments, related to each wall configuration, have been divided by M_G^V , M_W^V , M_T^V , which are the average global, wall and trunk moments, respectively, obtained for the flushed wall configuration (G_{c1}) in the considered test. Thus, Figs. 6 and 7 provide a direct comparison, in terms of percentage force and moment increase/reduction, with the flushed wall configuration.

In Figs. 6 and 7, full black, gray, red and blue dots refer to G_{c1} (flushed wall), G_{c2} , G_{c3} , and G_{c4} , respectively. Furthermore, in Fig. 6

black dashed lines represent the quantities $F_G^V/\max(F_G^V)$ (first column), $F_W^V/\max(F_W^V)$ (second column), $F_T^V/\max(F_T^V)$ (third column), being $\max(F_G^V)$, $\max(F_W^V)$, and $\max(F_T^V)$ the maximum global, wall and trunk force values, respectively, measured during the most energetic wave test for the flushed wall configuration (G_{c1}). In Fig. 7 the same lines represent the quantities $M_G^V/\max(M_G^V)$ (first column), $M_W^V/\max(M_W^V)$ (second column), $M_T^V/\max(M_T^V)$ (third column), being $\max(M_G^V)$, $\max(M_W^V)$, and $\max(M_T^V)$ the maximum global, wall and trunk moment values, respectively, measured during the most energetic wave test for the flushed wall configuration (G_{c1}). Thus, these lines provide a measure, in terms of forces and moments, of the energetic content of each test.

Firstly, the global force (first column of Fig. 6) is considered. Considering low energy sea states (see panels a) and d)), the global force reduction is almost constant for the three wall retreat configurations (G_{c2} , G_{c3} and G_{c4}) and remains in the order of 10%. On the

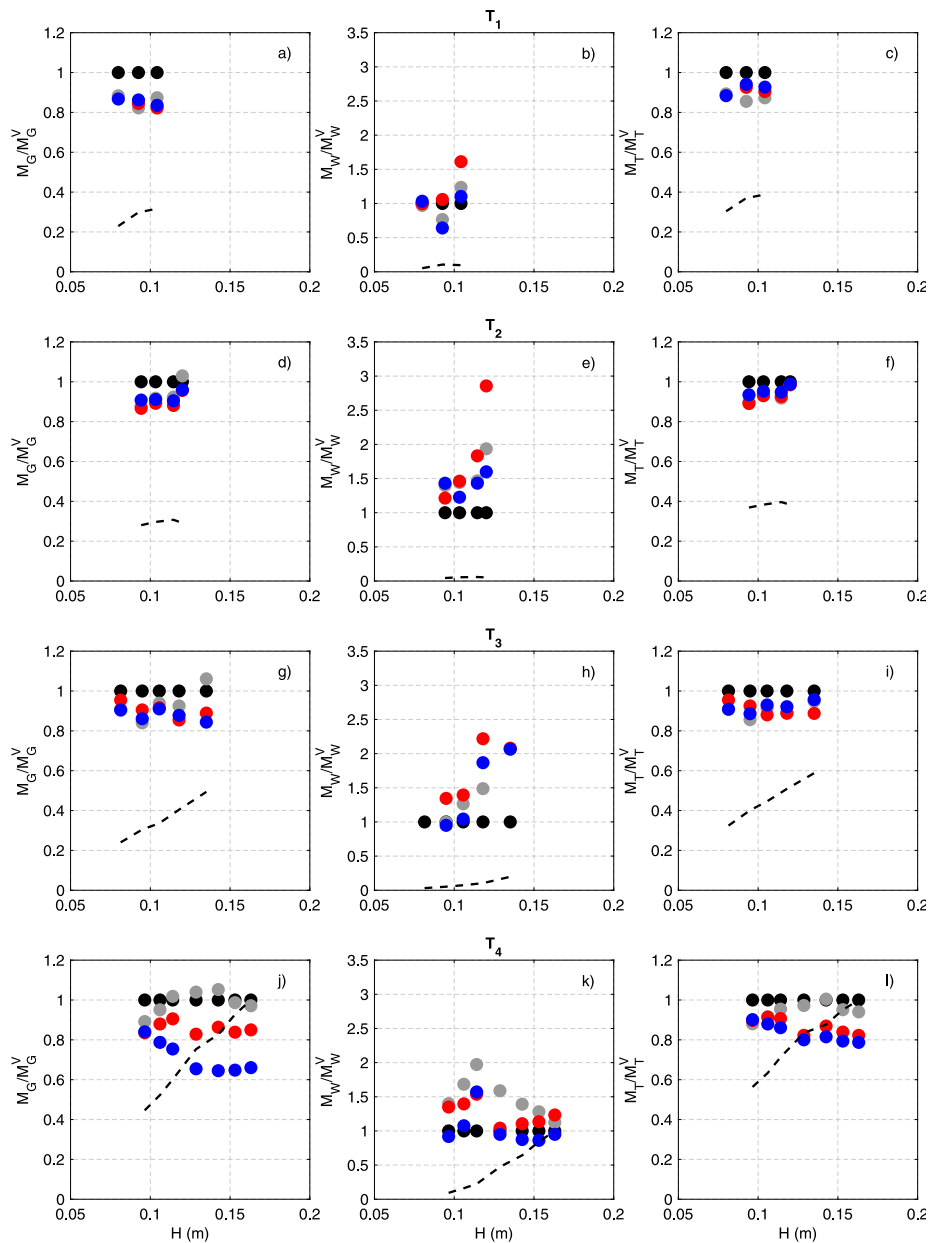


Fig. 7. Dimensionless global M_G/M_G^V , wall M_W/M_W^V , and trunk M_T/M_T^V moments as a function of the wave height for the four wall configurations. Note: each row refers to a different wave period (first, second, third, and fourth rows refer to T_1 , T_2 , T_3 , and T_4 , respectively), while each column refers to a different torque component acting on the structure (first, second, and third columns refer to the global, wall and trunk moments, respectively). Full black, gray, red, and blue dots refer to G_{c1} (flushed wall), G_{c2} , G_{c3} , and G_{c4} , respectively. Black dashed lines represent $M_G^V/\max(M_G^V)$ (first column), $M_W^V/\max(M_W^V)$ (second column), $M_T^V/\max(M_T^V)$ (third column).

contrary, if high energy sea states are considered (see panels *g*) and *j*)), a different behavior of the global force reduction between the wall configurations is evident. For small values of the wall retreat (G_{c2}) the percentage global force reduction is small (around 5%), negligible in some cases, while for large values of the wall retreat (G_{c3} and G_{c4}) the percentage global force reduction is significant and progressive (almost linearly decreasing with increasing wave heights), exhibiting a maximum percentage reduction of 17% for G_{c3} and 31% for G_{c4} , respectively.

Loads on the wall (second column of Fig. 6) experience a general increase for the three wall retreat configurations (G_{c2} , G_{c3} and G_{c4}). Considering the less energetic sea states (see panels *b*) and *e*)), the wall force increase is very significant, reaching values of 200% (300% in one case), while if highly energetic sea states are considered (see panels *h*) and *k*)), again, a different behavior between the wall configurations is evident. The percentage wall force increase is significant for the wall

configurations G_{c2} and G_{c3} , exhibiting values in the range 25%–50%, while for the wall G_{c4} the wall force increase is very small, negligible in some cases. Furthermore, it is important to stress, that the wall retreat may change the nature of the loads acting on the wall itself. In fact, the flushed wall configuration experiences, as expected, pulsating loads, while for the three wall retreat configurations (G_{c2} , G_{c3} and G_{c4}) impulsive loads (i.e., church-roof-like impacts) occur. This is further discussed later.

As far as the trunk forces are concerned (third column of Fig. 6), a similar behavior of what discussed for global forces can be noticed. Looking at the highly energetic sea states (see panels *i*) and *l*)), for the configuration G_{c2} the percentage trunk force reduction is around 7%, negligible in some cases, while for the configurations G_{c3} and G_{c4} , this reduction is significant and progressive (almost linearly decreasing with increasing wave heights as shown for the global forces), exhibiting

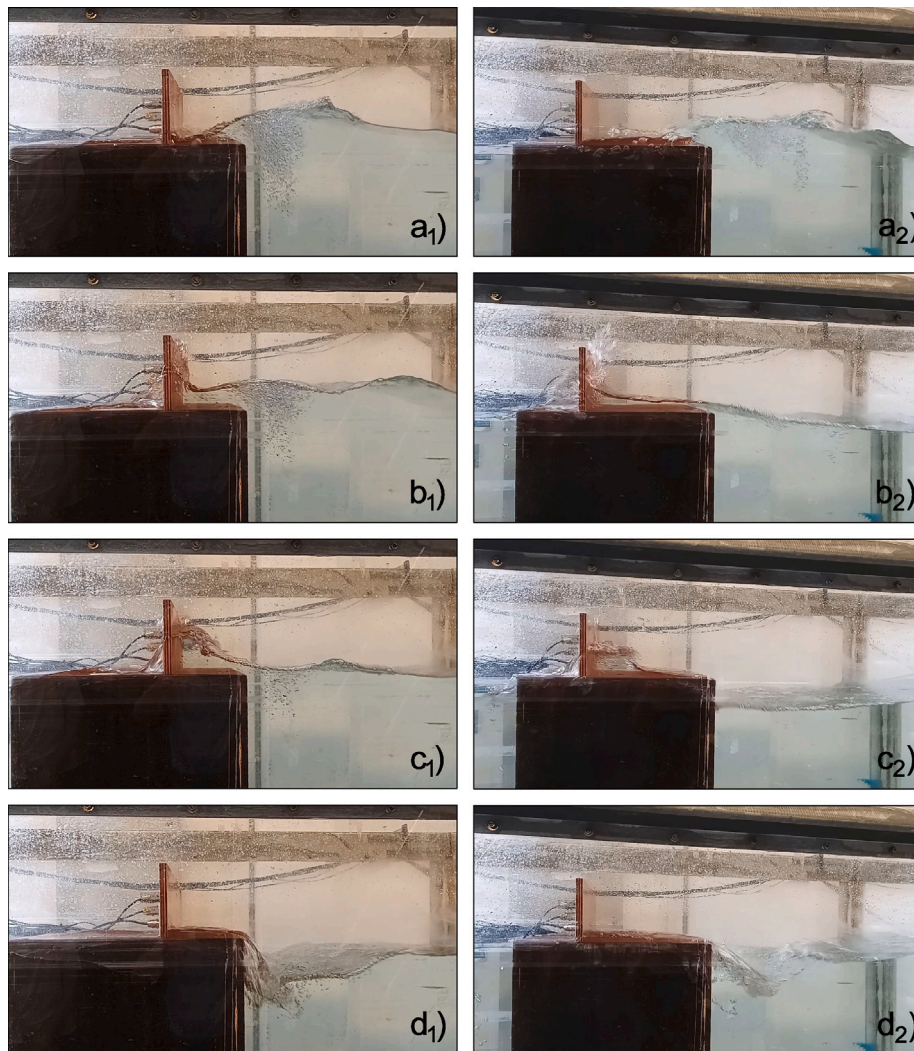


Fig. 8. Visual evolution of the wave-structure interaction phenomena over one wave period at four selected time instants for two retreated wall configurations (G_{c3} , first column and G_{c4} , second column).

a maximum percentage reduction of 19% for G_{c3} and 21% for G_{c4} , respectively.

Very similar considerations arise if the moments are considered (Fig. 7). The global moment reduction (first column of Fig. 7) is almost constant, in the order of 15%, for the three wall retreat configurations for low energy sea states (see panels *a*) and *d*)). On the contrary, as pointed out considering the forces, for higher energetic sea states (see panels *g*) and *j*)), a different behavior of the global moment reduction between the wall configurations is evident. For the small wall retreat (G_{c2}) the percentage global moment reduction is small (around 7%), negligible in some cases, while for large values of the wall retreat (G_{c3} and G_{c4}) the percentage global force reduction is exhibiting a maximum percentage reduction of 15% for G_{c3} and 34% for G_{c4} , respectively.

Also considering the moments acting of the caisson wall and trunk (second and third columns of Fig. 7, respectively), the analysis confirms the findings already discussed for the forces (see Fig. 6). In fact, the moments on the wall experience a general increase, which is similar, in magnitude and behavior, to that experienced by the forces. In the same way, the moments on the caisson trunk are characterized by a pattern very similar to that already described for the global moments: i.e., small/negligible reduction for small wall retreat (G_{c2}) and significant reduction for large values of the wall retreat (18% for G_{c3} and 22% for G_{c4} , respectively).

In order to better understand the physical/geometrical drivers that play a role on the force increase/reduction behavior as a function of

the wall position, a detailed analysis of the wave-structure interaction physics is presented and discussed in the following of this section. In order to do this, the physics of the wave-structure interaction is firstly qualitatively described, looking at the visual evolution of the phenomena that occur over one wave period. Thus, Fig. 8 is presented. In this figure four selected time instants of the wave-structure interaction for two retreated wall configurations (G_{c3} , first column and G_{c4} , second column), over one wave period, are presented.

The panels of the first row of Fig. 8 show the approach phase of the wave front. The rising wave crest, which is climbing on the caisson trunk, overtops the seaside edge of the caisson and a steep wave front/bore starts to propagate on the promenade towards the retreated wall (see panels *a*₁) and *a*₂)). Looking at those panels, it is possible to see that, for both wall configurations, a large number of air bubbles are trapped by the wave front that propagates towards the wall. Thus, the wave front exhibit a high degree of air entrainment. The reason of such air entrainment will be clear later on, when the panels *d*) of the same figure are described.

When the steep wave front/bore reaches the retreated wall an impact takes place (see panels *b*₁) and *b*₂)). Looking at those panels it appears that the nature of the impact, or in other words its degree of impulsivity, is intimately related to both the properties of the waves (e.g., wave height H and wave period T , wave nonlinearity, wave steepness, etc.) and the geometrical parameters (e.g., length of the

promenade G_c , wall height h_w , etc.). It is useful, in view of the following analyzes, to qualitatively discuss the nature of the impact only focusing on the relative positions between the two wall configurations considered in the picture. In fact, for the considered wave condition, an “intermediate” wall retreat (G_{c3} , panel b_1) seems to result in a less impulsive nature of the impact. In fact, the water front hitting the wall is compact and sustained by the wave which is still climbing the caisson trunk, thus hypothesizing a negligible time shifting between the instants at which the maximum loads on the caisson trunk and wall take place. On the other hand, a “large” wall retreat (G_{c4} , panel b_2) seems to result in a higher degree of impulsivity of the water front hitting the wall. In the picture it is clearly visible the vertical water jet produced by the impact with the wall. The highly retreated wall position allows the water layer, that in the initial phase of its propagation accelerates on the promenade, to spread during its run towards the wall itself, resulting in a thinner water layer that resembles the front evolution of a dam break. Moreover, this water front, although propagating very quickly, is not feeded/sustained by the wave crest in front of the caisson, which indeed already started its descending phase towards the following trough phase. This aspect allows to hypothesize that, in this configuration, the time shifting between the instants at which the maximum loads on the caisson trunk and wall can play an important role.

All these qualitative considerations seem to be confirmed looking at the next time instants (see panels c_1 and c_2) depicted in Fig. 8. Here, the water mass after the impact with the wall is reflected by the wall itself and starts its backwash phase. Again, at least for the considered experimental conditions, depending on the wall position (and of course on the wave properties) there is continuity (G_{c3} , panel c_1) or not (G_{c4} , panel c_2) between the water mass on the promenade and the wave acting on the caisson trunk. For G_{c3} the wave acting on the trunk started now its descending phase, while for G_{c4} the descending phase of the wave is already well developed, resulting in a clear detachment/separation with the water mass which is backwashing on the promenade.

The backwash phase of the water mass ends with a water jet that, flowing from the promenade, flushes from the seaside edge of the caisson and plunges into water (see panels d_1 and d_2). These plunging jets increase the air entrainment in the flow (see panels a_1 and a_2) and, at the same time, increase the turbulence in front of the structure, causing those fluctuations already highlighted in the pressure signals of Fig. 5. Note that, depending on the wall position, the shape and the angle of the plunging jet can vary significantly. In fact, for G_{c3} (see panel d_1) the plunging jet is subvertical and relatively weak, while for G_{c4} (see panel d_2) the jet is subhorizontal and very impetuous. Moreover, hitting the water surface at a certain distance from the caisson and pointing seaward with a subhorizontal trajectory it is able to interact significantly with the next incoming wave, disturbing the wave field and increasing the turbulent dissipations.

The wave-structure interaction dynamic shown in Fig. 8 has been qualitatively analyzed only for one single wave condition and two wall configurations. However the physical phenomena that take place can be easily identified and can be used to guide the interpretation of the force increase/reduction as a function of the wall position presented in Fig. 6. In fact, the physical phenomena that take place in the wave-structure interaction dynamics for retreated wall are always similar among different wall positions, while the effect of these phenomena on the wave loads can significantly change depending on the distance of the wall from the edge of the caisson.

Specifically, these wave-structure interaction phenomena suggest that several physical/geometrical drivers play a role on the force increase/reduction for retreated wall configurations, namely: I) time shifting between impacts on caisson trunk and wall; II) unloading of the water column acting on the trunk due to overtopping of the seaside edge of the caisson; III) increase of the forces on the wall due

to occurrence of impulsive loads. All these aspects are now carefully analyzed.

In order to analyze the time shifting between impacts on caisson trunk and wall and, accordingly, the nature of the impacts themselves, as a function of the wave and geometrical characteristics, Figs. 9, 10, 11, and 12 are presented. All these figures, each referring to different wave periods (Figs. 9, 10, 11, and 12 refer to T_1 , T_2 , T_3 , and T_4 , respectively) and wave height (from mild to severe) conditions, present four panels each. Each panel refers to a different wall configuration (first, second, third, and fourth panels refer to G_{c1} , G_{c2} , G_{c3} , and G_{c4} , respectively). In all the panels two pressure signals are represented, namely: the pressure signals measured by the upper sensor of the trunk (P_7 , dashed gray lines); the pressure signals measured by the lowest sensor of the wall (P_8 , continuous black lines).

In all the figures it is clear that, as expected, for the flushed wall configuration G_{c1} , the pressure signals P_7 and P_8 are perfectly in phase (first panels of Figs. 9, 10, 11, and 12). Thus, regardless the wave characteristics, the maximum value of the pressure signals occur simultaneously on caisson trunk and wall; as expected there is no time shifting between impacts on caisson trunk and wall. On the contrary, for retreated wall configurations the timing of those impacts depends on both wave characteristics and wall position. Looking at very mild sea states (Figs. 9 and 10) there is a significant time lag between the impacts on the wall and on the trunk for the wall configurations G_{c3} , and G_{c4} , while it is less pronounced for G_{c2} , although, as stated, these wave conditions induce very mild loads on both trunk and wall. On the other hand, looking at more energetic sea states (Figs. 11 and 12) very different behavior occur as a function of the wall position. For G_{c2} and G_{c3} it can be seen that time shifting between the impacts on the wall and trunk is almost negligible. Furthermore, the nature of the impacts on the wall is impulsive (i.e., church-roof-like pressure time series), as shown in Fig. 13, that provides an example of the most violent pressure signal measured for G_{c4} .

Moreover, in some cases (e.g., G_{c2}) the peak of the impact on the wall anticipates the maximum load on the trunk, then exhibiting a quasi-static load when the latter occurs. As far as G_{c4} is concerned, it can be seen that a significant time shifting always occurs between the maxima load instants on wall and trunk. Nevertheless, as inferred from Fig. 8, the nature of the loads on the wall is strongly impulsive, indeed the peak of the church-roof-like impact is very pronounced. Another interesting aspect, that arises during the more energetic sea states (Figs. 11 and 12), is that the measured signals at the wall often exhibit a double peak with the second peak being at times higher and at times lower with respect to the first one. This behavior is probably due to the complex nature of the hydrodynamics and the impulsive impacts. In fact, depending also on the mutual combination of wave condition and the wall configuration, the first peak is related to the impulsive impact induced by the wave front/bore, while the second peak (if present) is related to the quasi-static load induced by the water mass that follows the wave front/bore. It is well known that impulsive impacts are highly localized both in space and time. Thus, under certain flow conditions and wall configurations, small variations on the wave-structure interaction hydrodynamics could affect the nature and/or the measurement of the first peak, which results at times higher and at times lower with respect to the second one. Furthermore, as this is a turbulent post-overtopping process, the incoming wave front/bore is affected by the hydrodynamic effects induced by the backwash flow on the promenade.

These considerations are well supported by Fig. 14, where the quantitative analysis of the time lags between the occurrence of the maximum pressure on the trunk and on the wall are reported. As previously stated, the horizontal force signals (F_G , F_W and F_T), obtained through the integration of the pressure signals, have been processed by means of a peaks over threshold (POT) analysis to identify the force peaks within the above mentioned time window. Thus, for each test, the time lags Δt_i , each defined as the difference between the time

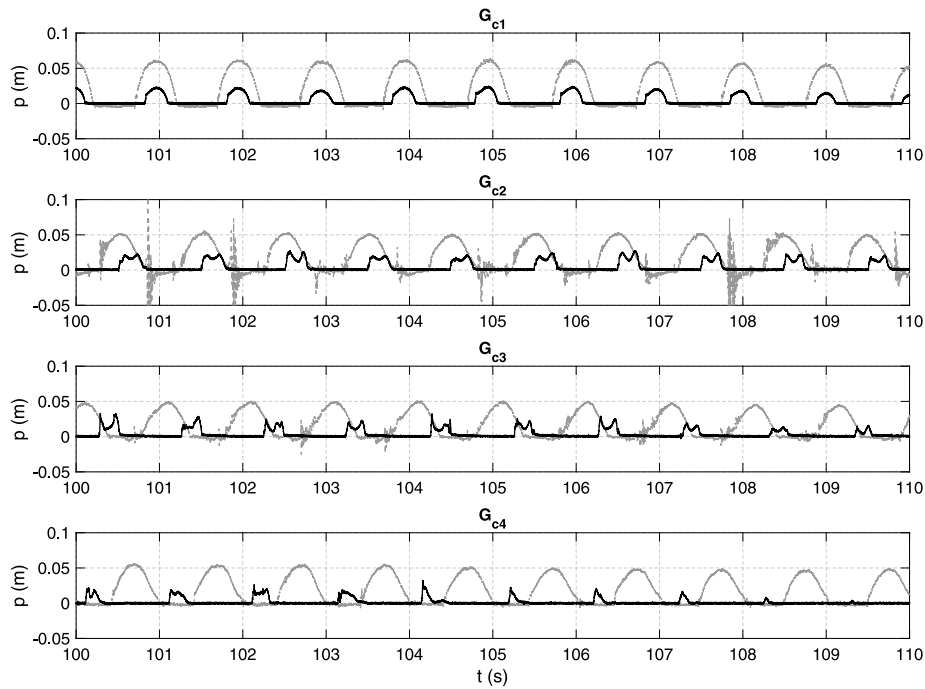


Fig. 9. Pressure signals measured by the uppest sensor of the trunk (P_7 , dashed gray lines); the pressure signals measured by the lowest sensor of the wall (P_8 , continuous black lines) under the wave period $T = 0.10$ s). Note: each panel refers to a different wall configuration (first, second, third, and fourth panels refer to G_{c1} , G_{c2} , G_{c3} , and G_{c4} , respectively).

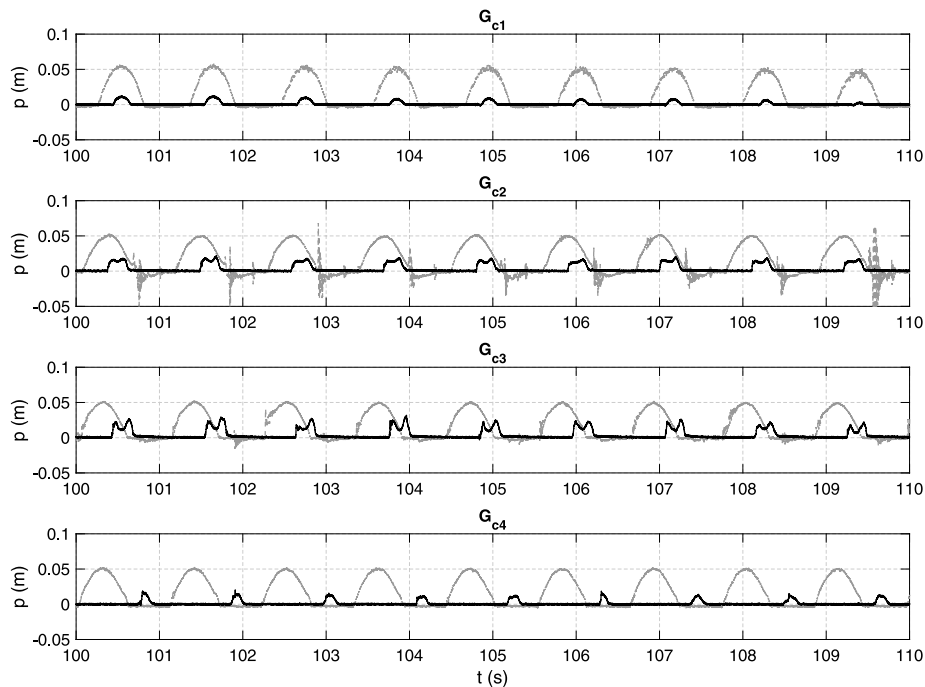


Fig. 10. Pressure signals measured by the uppest sensor of the trunk (P_7 , dashed gray lines); the pressure signals measured by the lowest sensor of the wall (P_8 , continuous black lines) under the wave period $T = 0.11$ s). Note: each panel refers to a different wall configuration (first, second, third, and fourth panels refer to G_{c1} , G_{c2} , G_{c3} , and G_{c4} , respectively).

instants at which maximum load values on wall and caisson trunk, respectively, occur, have been obtained. Since regular waves have been used, average values of these time lags over the time window have been obtained and divided by the considered wave period ($\overline{\Delta t}/T$) to make them dimensionless. Note that each panel of Fig. 14 refers to a different wave period and the usual color code is used for the markers. Fig. 14 confirms and extends what inferred looking at the Figs. 9,

10, 11, and 12. The time shifting between impacts on caisson trunk and wall, and accordingly the nature of the impacts themselves, is intimately dependent on both wave and geometrical characteristics. It is important to stress that for certain wall positions (G_{c2} and G_{c3}) and wave conditions tested in this campaign, the time shifting between the impacts on the wall and trunk is almost negligible (see lower right panel of Fig. 14).

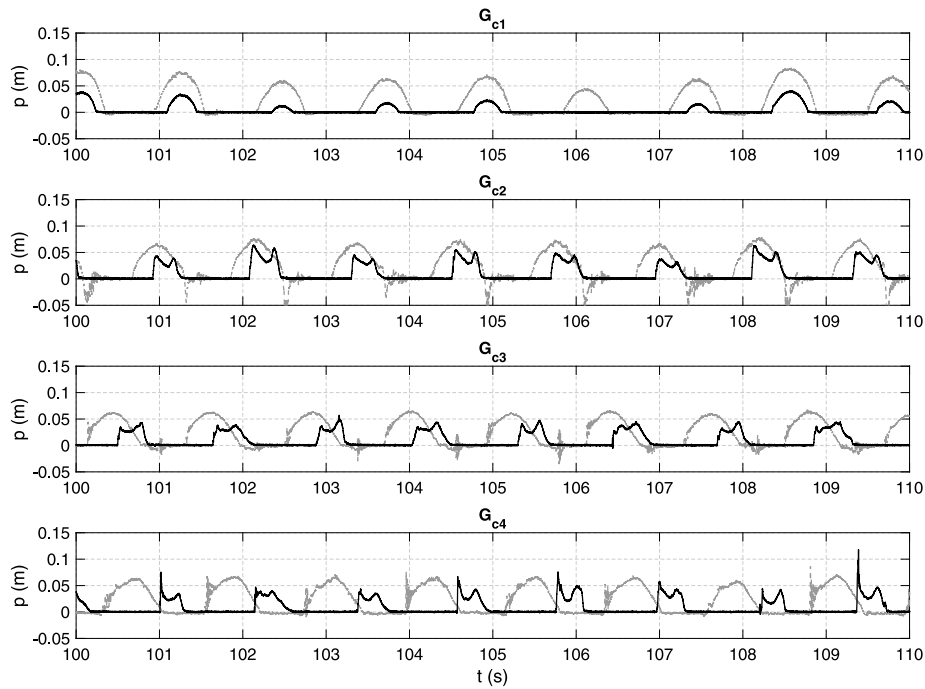


Fig. 11. Pressure signals measured by the uppest sensor of the trunk (P_7 , dashed gray lines); the pressure signals measured by the lowest sensor of the wall (P_8 , continuous black lines) under the wave period $T = 0.12$ s. Note: each panel refers to a different wall configuration (first, second, third, and fourth panels refer to G_{c1} , G_{c2} , G_{c3} , and G_{c4} , respectively).

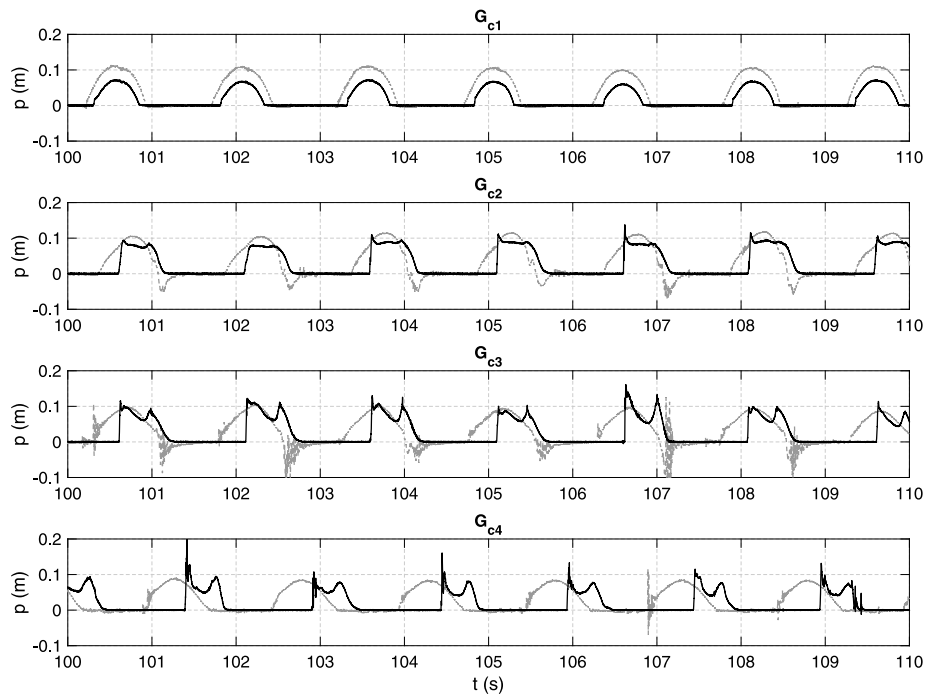


Fig. 12. Pressure signals measured by the uppest sensor of the trunk (P_7 , dashed gray lines); the pressure signals measured by the lowest sensor of the wall (P_8 , continuous black lines) under the wave period $T = 0.15$ s. Note: each panel refers to a different wall configuration (first, second, third, and fourth panels refer to G_{c1} , G_{c2} , G_{c3} , and G_{c4} , respectively).

Finally, the driver related to the unloading of the water column acting on the trunk due to overtopping of the seaside edge of the caisson is explored. The rising wave that overtops the seaside edge of the caisson, starting to propagate as a bore on the promenade towards the wall, causes a lightening/unloading mechanism of the water column acting on the caisson trunk. Again, this unloading mechanism is expected to be influenced by both wave and geometrical characteristics.

To better understand this mechanism, Fig. 15 is presented. In this figure, each panel refers to a different wave condition (being the first panel related to a mild wave condition, wave period T_1 , and the fourth to the more energetic one, wave period T_4). In each panel the pressure signals measured by the uppest sensor of the caisson trunk (P_7) for the four wall configurations (continuous black, gray, red, and blue lines for G_{c1} , G_{c2} , G_{c3} , and G_{c4} , respectively) are reported. Looking at mild sea

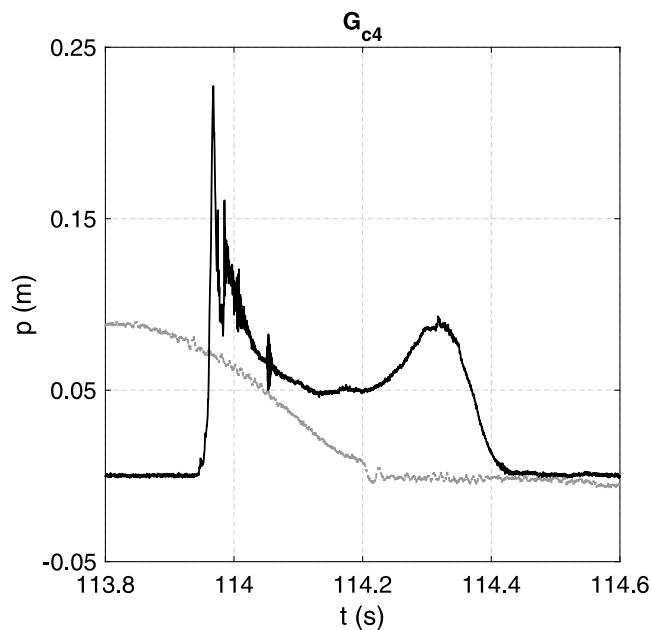


Fig. 13. Zoom of the pressure signals measured by the uppermost sensor of the trunk (P_t , dashed gray lines) and the lowest sensor of the wall (P_b , continuous black lines) under the wave period $T = 0.15$ s during the most violent wave impact of the time series (wall configuration G_{c4}).

states the unloading mechanism, regardless the wall position, seems to be play a negligible role. On the contrary, as far as highly energetic sea states are concerned (fourth panel of Fig. 15), the contribution of this mechanism is remarkable and strongly depends on the wall position. In fact, for a “small” wall retreat (G_{c2}) no significant differences in the pressure signals can be detected if compared with those obtained for the flushed wall configuration (G_{c1}). While, larger wall retreats may cause large (G_{c3}) and/or very large (G_{c4}) unloading of the water column acting on the trunk, reaching a maximum percentage decrease of 25% for G_{c4} , thus confirming what inferred from Fig. 8 (see panels c_1) and c_2).

To summarize, this synchronous analysis of the forces, used to enucleate the basic physical phenomena involved and to identify the physical/geometrical drivers, which are expected to play a role on the force increase/reduction as a function of the wall position, showed a crucial aspect which is worth to be highlighted. Indeed, these physical/geometrical drivers, can have both a concordant and antithetical action among them, then resulting in increasing or decreasing, respectively, forces acting on the structure.

3.4. Pressures: Asynchronous analysis

In this section the asynchronous analysis of the pressures on the structure is carried out. For each pressure transducer the maximum value, recorded in the considered time window, is stored and used to build a diagram showing how the pressure changes along the structure. Of course, the pressure levels, might occur at different times.

Thus, for each experiment average values of the pressure peaks, each referring to a different vertical coordinate, have been obtained for the four wall configurations. An example of these values for six sea states (spanning from mild to high energy) are reported in Figs. 16, 17, and 18 in the form of pressure diagrams. In the figures, experimental pressure diagrams are represented by continuous black, gray, red, and blue lines with markers for G_{c1} , G_{c2} , G_{c3} , and G_{c4} , respectively, while dotted red lines represent the theoretical pressure diagrams as from the Goda’s formulae (Goda, 2010). Finally, also the caisson (filled gray), the rubble mound foundation (filled yellow), and the still water level

(horizontal dashed blue lines) are represented in the figure. Note that, although the experimental pressure diagrams refer to the four wall configurations, only the flushed wall configuration caisson is sketched in the figures for visualization purposes.

Figs. 16, 17, and 18 confirm and extend what inferred in the synchronous analysis of the forces. In fact, considering mild/moderate wave conditions (see Figs. 16 and 17) the global loading increase (if any), if compared with the loading condition occurring for the flushed wall configuration (G_{c1}), is only due to the increasing loading on the wall, although potentially shifted in time with respect to the loads on the trunk. In fact, for these wave conditions, the unloading on the caisson trunk is negligible, regardless the wall position. On the other hand, for highly energetic wave conditions (see Fig. 18, panel b)), it is possible to see a significant difference between the experimental pressure diagrams related to retreated and flushed wall configurations and also large differences among pressure diagrams related to different wall retreats.

For “large” wall retreats (G_{c4}), and highly energetic sea states, it is noticeable an increasing loading on the wall, which nevertheless is significantly shifted in time with respect to the loading on the trunk, as demonstrated by the signals in Figs. 11 and 12, and a pressure distribution on the caisson trunk significantly unloaded, if compared with that occurring for the flushed wall configuration, along the trunk itself. Thus, the global loading conditions for this caisson configuration is significantly lower than that experienced for the flushed wall configuration under the same wave conditions.

For “intermediate” wall retreats (G_{c3}), and highly energetic sea states, it is again noticeable an increasing loading on the wall, which in this case may be not significantly shifted in time with respect to the peak acting on the trunk, see Figs. 11 and 12, and a pressure distribution on the caisson trunk significantly unloaded along the trunk itself, with a vertical distribution very similar to that of G_{c4} . Thus, the global loading conditions for this caisson configuration is globally lower than that experienced for the flushed wall configuration under the same sea states.

Finally, for “small” wall retreats (G_{c2}), and highly energetic sea states, it is noticeable an increasing loading on the wall, which for this wall configuration is almost in phase or at least not significantly shifted in time with respect to the trunk, see Figs. 11 and 12, and a pressure distribution on the caisson trunk which exhibits a poor/negligible degree of unloading due to the overtopping on the edge: the vertical distribution of the pressure is indeed very similar to that occurring for the flushed wall configuration. Thus, the loading condition for this caisson configuration is globally equal/higher than that experienced for the flushed wall configuration under the same sea state. To summarize, this caisson configuration, at least under the tested wave conditions, does not introduce any advantage in terms of loading reduction. On the contrary, while on the trunk very similar loading conditions to those of the flushed wall configuration occur, the wall is under impulsive loading conditions, almost in phase with those acting on the rest of the caisson. It results that caissons with “small” wall retreat experience larger loads than standard flushed wave wall structures.

3.5. Force increase/reduction factor

As stated, this paper aims at presenting a first experimental insight on the physics behavior of the force increase/reduction acting on an ideal composite vertical breakwater with retreated wall. Nevertheless, the experimental evidence presented so far, can be used as base to provide in the future, with more analysis and further investigation (both physical and numerical modeling), design guidelines or recommendations for this technical solution. With this in mind, in this section, a preliminary analysis to calculate dimensionless force increase/reduction factors, based on the experimental evidences described so far, is presented. The analysis is divided into two parts with two different purposes: I) to test the goodness of a potential

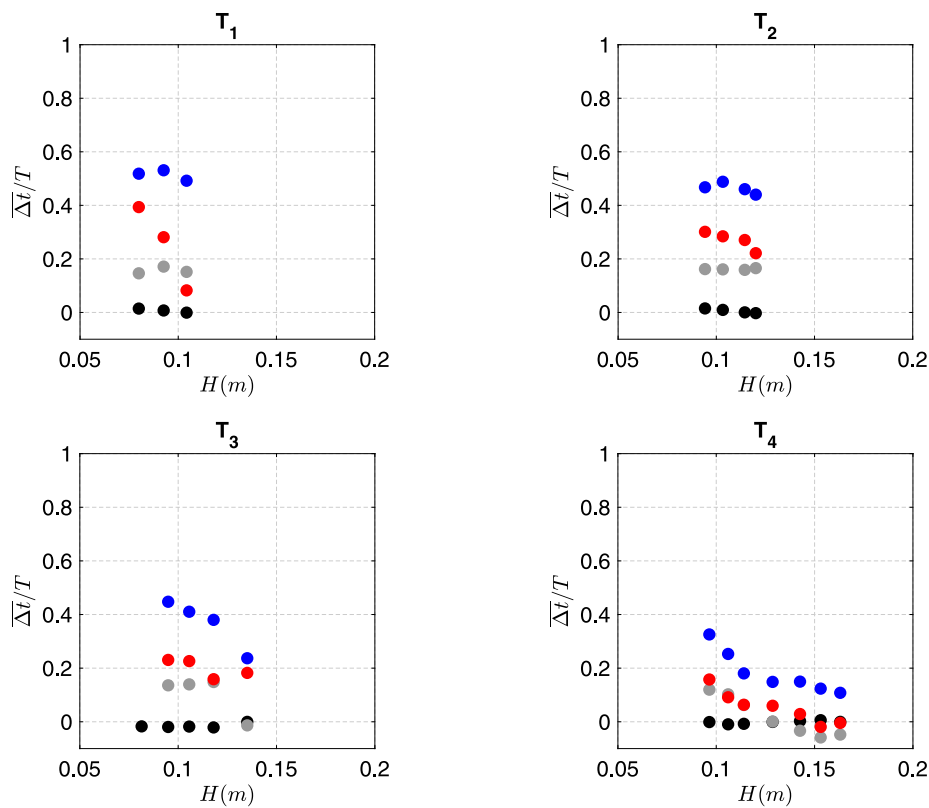


Fig. 14. Dimensionless time lags between impacts on caisson trunk and wall as a function of the wave height and wave period ($T_1 = 1.0$ s, upper left panel; $T_2 = 1.1$ s, upper right panel; $T_3 = 1.2$ s, lower left panel; $T_4 = 1.5$ s, lower right panel). Note: black dots refer to the flushed wall configuration (G_{c1}), while gray, red, and blue dots refer to G_{c2} , G_{c3} , and G_{c4} , respectively.

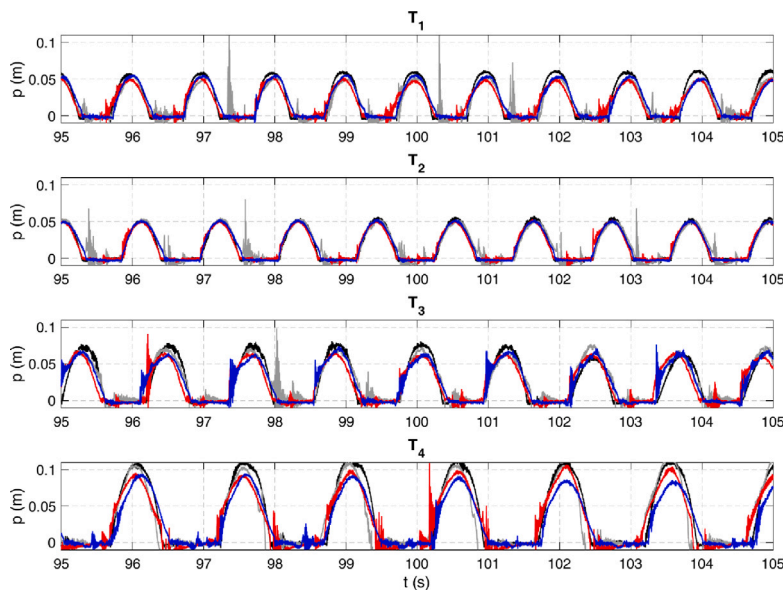


Fig. 15. Pressure signals measured by the uppest sensor of the caisson trunk (P_7) for the four wall configurations (continuous black, gray, red, and blue lines for G_{c1} , G_{c2} , G_{c3} , and G_{c4} , respectively). Note: each panel refers to a different wave condition (being the first panel related to a mild wave condition, wave period T_1 , and the fourth to the more energetic one, wave period T_4).

explanatory variable to estimate the global forces as a function of wall position and wave conditions; II) to provide a preliminary estimate of the force increase/reduction factor, with respect to the flushed wall configuration, as a function of the wall position and wave conditions.

For the first purpose reference is made to Fig. 19. The dimensionless averaged global forces $F_G/\rho gh^2$ are plotted as a function of

the potential explanatory variable $\frac{H}{h} \frac{L_0}{h} \left(\frac{L_0 - G_c}{L_0} \right)^2$. It is worth noticing that the potential explanatory variable is based on simple heuristic interpretations of the physical phenomena involved, trying consider the following aspects: (I) the strong dependence with the wave height; (II) the effect of the wave nonlinearity (H/h) and wave frequency dispersiveness (h/L_0); (III) the importance of relative distance between

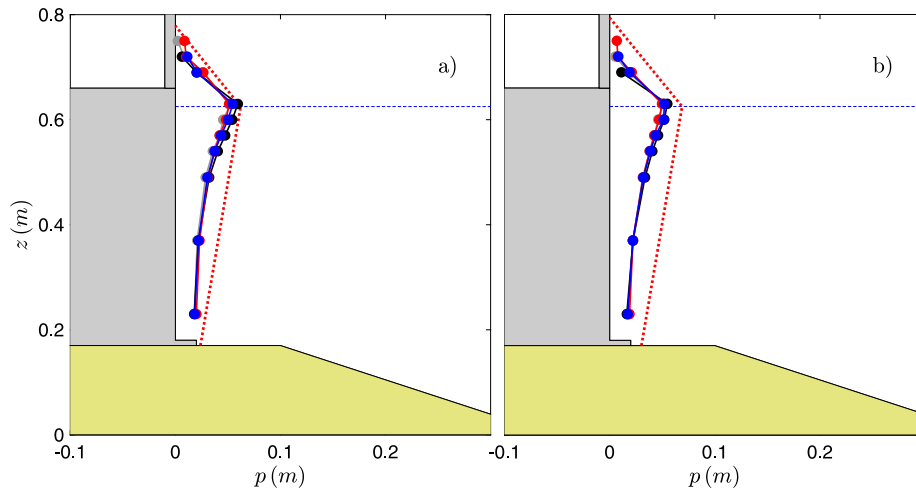


Fig. 16. Pressure diagrams for the four wall configurations under two mild energy sea states. Note: experimental pressure diagrams are represented by continuous black, gray, red, and blue lines with markers for G_{c1} , G_{c2} , G_{c3} , and G_{c4} , respectively, while dotted red lines represent the pressure diagrams as from the Goda's formulae (Goda, 2010). The caisson (only the flushed wall configuration caisson is sketched in the figure for visualization purposes with filled gray), the rubble mound foundation (filled yellow), and the still water level (horizontal dashed blue lines) are also represented.

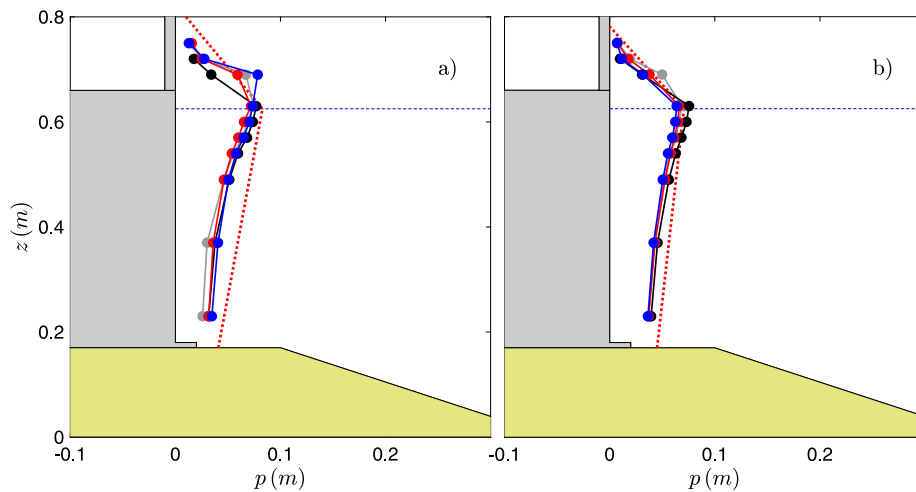


Fig. 17. Pressure diagrams for the four wall configurations under two moderate energy sea states. Note: experimental pressure diagrams are represented by continuous black, gray, red, and blue lines with markers for G_{c1} , G_{c2} , G_{c3} , and G_{c4} , respectively, while dotted red lines represent the pressure diagrams as from the Goda's formulae (Goda, 2010). The caisson (only the flushed wall configuration caisson is sketched in the figure for visualization purposes with filled gray), the rubble mound foundation (filled yellow), and the still water level (horizontal dashed blue lines) are also represented.

G_c and the wavelength. Note that the usual color code is used for the markers. Fig. 19 shows that the data obtained under these experimental conditions, for different wall configurations, are well grouped and seem to follow a linear relationship for increasing values of the proposed explanatory variable.

In order to further extend this part of the analysis, the forces acting separately on the caisson trunk and wall are plotted in Fig. 20. Here, $\frac{F_G}{\rho g h^2}$, $\frac{F_T}{\rho g h^2}$, and $\frac{F_W}{\rho g h^2}$, obtained in all the experimental tests and for all the wall configurations, are represented with empty black, full blue, and full red dots, respectively. The tested explanatory variable is suitable to represent the behavior of the forces acting on the caisson trunk and wall, which exhibit a linear and slightly nonlinear behavior, respectively, for increasing values of the explanatory variable. As expected, considering mild wave conditions, the contribution of the forces acting on the wall on the global force is negligible, as the global force is almost totally composed by the force acting on the caisson trunk. While, for highly energetic sea states the contribution of the forces acting on the wall is significant. These considerations provide a further key to interpret the synchronous analysis of the forces as a function of the wall position previously presented.

In order to provide a preliminary estimate of the force increase/reduction factor, with respect to the flushed wall configuration, as a function of the wall position and wave conditions (i.e., the second purpose of the analysis), Figs. 21 and 22 are presented. In this case, the dimensionless variables $\frac{F_T}{F_T^V}$ (Fig. 21) and $\frac{F_G}{F_G^V}$ (Fig. 22) are plotted against the dimensionless parameter $\frac{H}{h} \frac{L_0}{h} \frac{G_c}{h_w}$. Note that the usual color code is used for the markers. Dashed black lines refers to the best fitting of the experimental data. Furthermore, it is worth to stress that in order magnify the influence of the wall position on the force increase/reduction factor, only the most energetic sea states are considered for this analysis.

Figs. 21 and 22 clearly show that the experimental data lie on a linear descending pattern as a function of $\frac{H}{h} \frac{L_0}{h} \frac{G_c}{h_w}$, providing a good agreement with a linear interpolating curve, with $R^2 = 0.65$ for $\frac{F_T}{F_T^V}$ and $R^2 = 0.80$ for $\frac{F_G}{F_G^V}$. When $\frac{H}{h} \frac{L_0}{h} \frac{G_c}{h_w}$ is equal to 0 (i.e., flushed wall configuration), then $\frac{F_T}{F_T^V}$ and $\frac{F_G}{F_G^V}$ are, consistently, equal to 1. Moreover, the slope of the reduction factor for global forces is more pronounced than that for forces acting on the caisson trunk. This is consistent

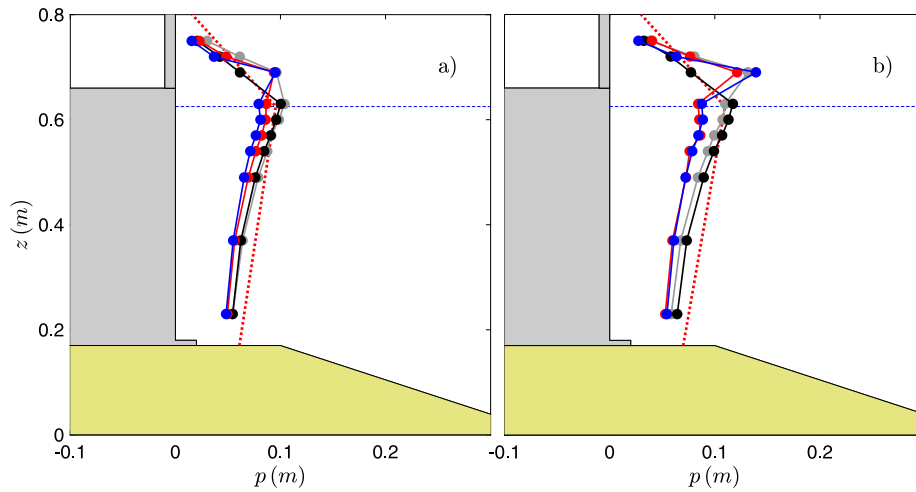


Fig. 18. Pressure diagrams for the four wall configurations under two high energy sea states. Note: experimental pressure diagrams are represented by continuous black, gray, red, and blue lines with markers for G_{c1} , G_{c2} , G_{c3} , and G_{c4} , respectively, while dotted red lines represent the pressure diagrams as from the Goda's formulae (Goda, 2010). The caisson (only the flushed wall configuration caisson is sketched in the figure for visualization purposes with filled gray), the rubble mound foundation (filled yellow), and the still water level (horizontal dashed blue lines) are also represented.

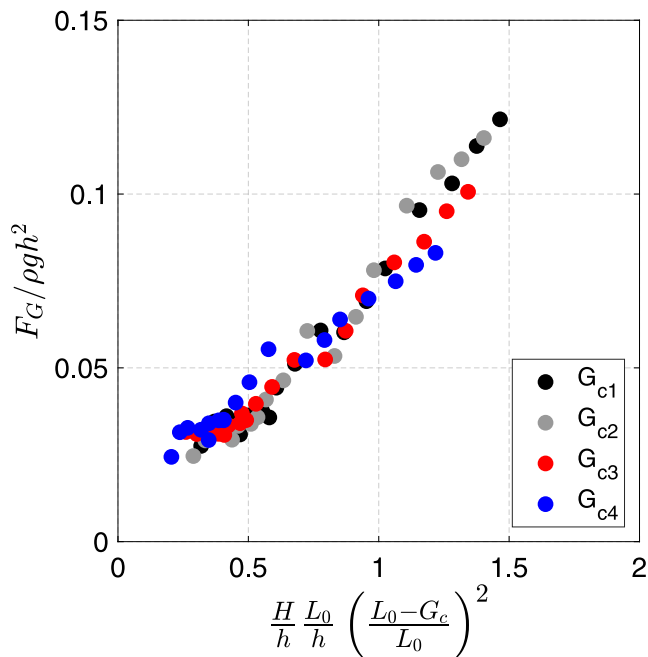


Fig. 19. Dimensionless averaged global forces $F_G / \rho g h^2$ as a function of the potential explanatory variable $\frac{H}{h} \frac{L_0}{h} \left(\frac{L_0 - G_c}{L_0} \right)^2$. Note: black dots refer to the flushed wall configuration (G_{c1}), while gray, red, and blue dots refer to G_{c2} , G_{c3} , and G_{c4} , respectively.

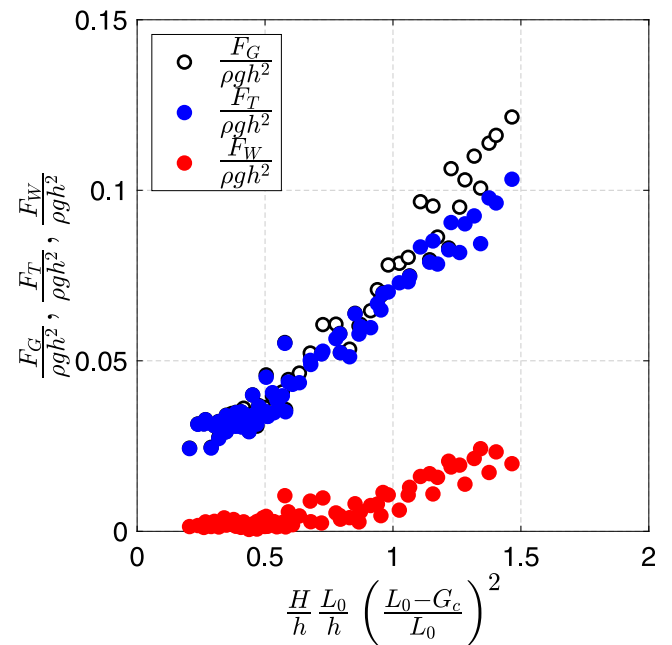


Fig. 20. Dimensionless global $\frac{F_G}{\rho g h^2}$ (empty black dots), trunk $\frac{F_T}{\rho g h^2}$ (full blue dots), and wall $\frac{F_W}{\rho g h^2}$ (full red dots) forces obtained in all the experimental tests and for all the wall configurations as a function of the potential explanatory variable $\frac{H}{h} \frac{L_0}{h} \left(\frac{L_0 - G_c}{L_0} \right)^2$.

considering the results discussed so far. Therefore, Figs. 21 and 22 provide, at least for the tested geometrical and wave conditions, a preliminary estimate of force increase/reduction factor, with respect to the flushed wall configuration, by using a retreated wall.

3.6. Limitations of the study

This paper focuses on the physical phenomena induced by using a retreated wall on an ideal composite vertical breakwaters. Thus, aiming at shedding light on this aspect, several assumptions/simplifications have been adopted, on purpose, during the design and preparation phases of the experimental campaign.

Firstly, only regular waves have been used. This choice has been made aiming at enucleating the basic physical phenomena involved and at investigating the physical/geometrical drivers, which are expected to play a role on the force increase/reduction factor, avoiding the uncertainty in the results interpretation induced by the randomness of a real sea state. The goodness of this choice is confirmed by the analysis of the results, which showed that the physical/geometrical drivers may have both a concordant and antithetical action among them. Nevertheless, the use of irregular/random sea states is mandatory to investigate the influence of wave sequencing (Romano et al., 2015; Williams et al., 2019) and to draw more general conclusions.

Secondly, the range of some crucial parameters (e.g., h , h_b , R_c , A_c , h_w), tested during the experiments, should be extended to better

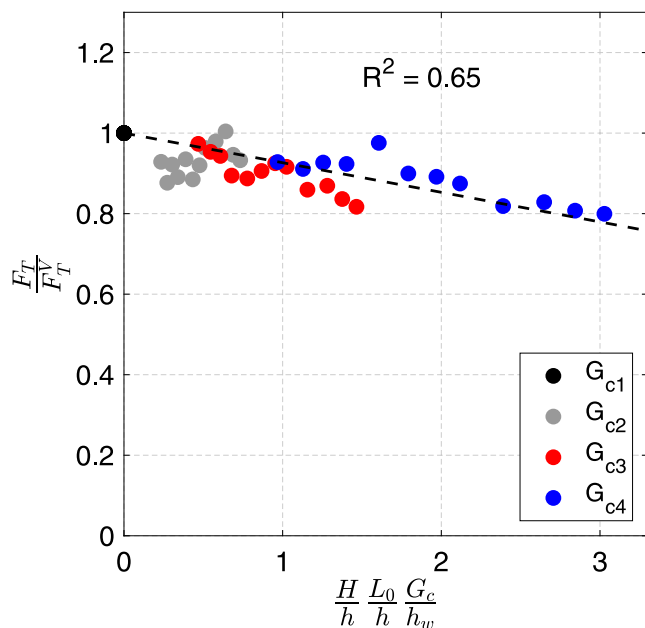


Fig. 21. Dimensionless force increase/reduction factor on the caisson trunk $\frac{F_T}{F_T^0}$ as a function of the dimensionless parameter $\frac{H}{h} \frac{L_0}{h} \frac{G_c}{h_w}$. Note: black dots refer to the flushed wall configuration (G_{c1}), while gray, red, and blue dots refer to G_{c2} , G_{c3} , and G_{c4} , respectively. Dashed black lines refers to the best fitting of the experimental data ($R^2 = 0.65$).

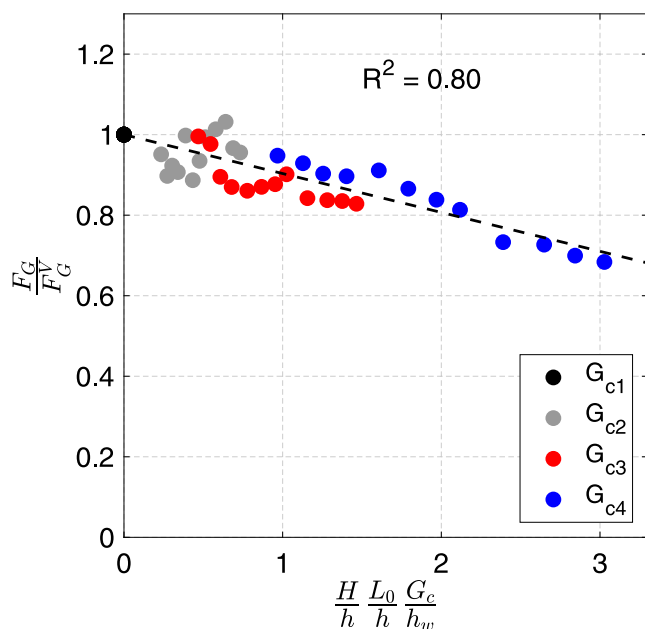


Fig. 22. Dimensionless global force increase/reduction factor $\frac{F_G}{F_G^0}$ as a function of the dimensionless parameter $\frac{H}{h} \frac{L_0}{h} \frac{G_c}{h_w}$. Note: black dots refer to the flushed wall configuration (G_{c1}), while gray, red, and blue dots refer to G_{c2} , G_{c3} , and G_{c4} , respectively. Dashed black lines refers to the best fitting of the experimental data ($R^2 = 0.80$).

explore their influence on the involved phenomena, in particular investigating the effects of the berm and wall height, which are expected to play a significant role, and to provide thorough design guidelines or recommendations for this technical solution.

Finally, in this study the influence of the wave overtopping at the crown wall has not been included. In fact, the wall height has been

specifically designed to avoid/limit the wave overtopping at the crown wall. This has been a precise choice adopted during the design of the experimental campaign, aiming at focusing on the “worst case scenario” for the forces acting on the caisson. In fact, it is expected that the wave overtopping may reduce the forces acting on the wall. Further investigation on the trade-off between acting forces and wave overtopping for a retreated wall configuration is needed in the future.

4. Conclusions

In this paper, the results of an experimental campaign aiming at shedding light on the influence, in terms of forces on the structure, of the crown wall position on top of an ideal composite vertical breakwater have been presented. The aim of this campaign is to provide a first experimental insight on the reduction/increase of the loads acting on the structure as a function of the retreat of the crown wall. To this end, four different wall retreat configurations (one flushed wall, G_{c1} , and three retreated wall configurations: G_{c2} , G_{c3} , and G_{c4}) have been investigated by using regular waves, by varying both wave height and wave period, to enucleate the basic physical phenomena involved and to investigate the physical/geometrical drivers, which are expected to play a role on the force increase/reduction factor. Thus, a detailed analysis of both forces (synchronous analysis) and pressures (asynchronous analysis) on the whole structure, the wall and the caisson trunk, have been measured and analyzed.

As a general result, the experimental evidences suggest that, at least for the four configurations tested, the global forces and moments acting on the caisson vary significantly depending on the wall position. Specifically, it appears that the global forces acting on the structure generally decrease as the wall retreat increases, with some dangerous exceptions, in which equal or larger loads, than those occurring for standard flushed wall configuration, are experienced by the structure. Apart from these exceptions, that deserve further investigation, almost for all the wall retreat configurations the global force experiences a reduction, which is in the order of 10% for low energy wave conditions, while it varies between 5% (G_{c2}) and 31% (G_{c4}) if high energy wave conditions are considered. Similar considerations and values can be done for the forces acting on the caisson trunk.

As far as forces acting on wave wall are considered, a general percentage force increase is noticed for all the wall retreat configurations, reaching extremely high values (up to 300%) for low energy wave conditions and smaller ones (in the range 25%–50%) for high energy wave conditions. Furthermore, during the experiments impulsive loads conditions on the wall occurred for all the wall retreat configurations. Moreover, a similar pattern, in magnitude and behavior, is found if the moments acting on the structure are considered.

These general considerations are supported and explained by the detailed analysis of the wave-structure interaction phenomena presented in the paper. In fact, this analysis suggested that several physical/geometrical drivers play a role on the force increase/reduction as a function of the wall position, namely: I) time shifting between impacts on caisson trunk and wall; II) unloading of the water column acting on the trunk due to overtopping of the seaside edge of the caisson; III) increase of the forces on the wall due to occurrence of impulsive loads. The synchronous analysis of the forces highlighted that these physical/geometrical drivers can have both a concordant and antithetical action among them, then resulting in increasing or decreasing, respectively, forces acting on the structure, if compared with the flushed wall configuration.

For “large” wall retreat (G_{c4}), and high energy sea states, it is expected an increasing loading on the wall, which nevertheless is significantly shifted in time with respect to the loading on the trunk, and a pressure distribution on the caisson trunk significantly unloaded, if compared with that occurring to the flushed wall configuration, along the trunk itself. Thus, the global loading conditions for this

caisson configuration is significantly lower than that experienced for the flushed wall configuration under the same sea states.

For “intermediate” wall retreat (G_{c3}) it is expected an increasing loading on the wall, which in this case may be not significantly shifted in time with the loading on the trunk, and a pressure distribution on the caisson trunk significantly unloaded along the trunk itself, with a vertical distribution very similarly to that of G_{c4} . Thus, the global loading conditions for this caisson configuration is globally lower than that experienced for the flushed wall configuration under the same sea states.

While, for “small” wall retreat (G_{c2}) it is expected an increasing loading on the wall, which for this wall configuration is almost in phase or at least not significantly shifted in time with the loading on the trunk, and a pressure distribution on the caisson trunk which exhibits a poor/negligible degree of unloading; indeed the vertical distribution of the pressure is very similar to that occurring for the flushed wall configuration. Thus, the global loading conditions for this caisson configuration is globally equal/higher than that experienced for the flushed wall configuration under the same sea states. To summarize, according to the results, this caisson configuration, under the tested wave conditions, does not imply any advantage in terms of loading reduction. On the contrary, on the trunk it is characterized by the same loading conditions obtained with a flushed wall configuration, but with the disadvantage of the impulsive loading conditions acting on the wall (almost in phase with those acting on the trunk).

Finally, it is worth to stress that, due to the complexity of the phenomena that take place, further research is needed. Specifically, as discussed in the limitations of the present study, it seems important to investigate the effect of irregular (random) wave conditions, to test more hydrodynamics and structural configurations and to support the physical modeling with numerical modeling, for instance by taking advantage of computational fluid dynamics (CFD) methods. Furthermore, it would be interesting to consider, in addition to the forces, the impulse and/or the force rise times; since the occurrence of impulsive loads is clearly reported, even for non-breaking wave conditions, considerations on structural dynamic response could arise. In fact, although the configuration used here is used in engineering practice, above all in retrofitting existing structures, it is not explicitly addressed in existing design parametric tools, therefore this study can provide some guidance and contribute to the development of future tools.

CRediT authorship contribution statement

Alessandro Romano: Conceptualization, Methodology, Investigation, Data curation, Formal analysis, Writing – original draft, Writing – review & editing, Software, Visualization. **Giorgio Bellotti:** Conceptualization, Methodology, Investigation, Formal analysis, Writing – review & editing, Funding acquisition.

Declaration of competing interest

The authors declare that they have no known competing financial interests or personal relationships that could have appeared to influence the work reported in this paper.

Data availability

Data will be made available on request.

Acknowledgments

A special acknowledgment is due to Eng. Giovanni Ercolani for the help provided during the experimental campaign.

References

- Aalborg University, A., 2018. Awasy7 [www document]. url www.hydrosoft.civil.aau.dk/awasy7.
- Andersen, T.L., Clavero, M., Eldrup, M.R., Frigaard, P.B., Losada, M., 2018. Active absorption of nonlinear irregular waves. In: Coastal Engineering 2018. Coastal Engineering Research Council.
- Andersen, T.L., Clavero, M., Frigaard, P., Losada, M., Puyol, J., 2016. A new active absorption system and its performance to linear and non-linear waves. *Coast. Eng.* 114, 47–60.
- Andersen, T.L., Eldrup, M.R., Frigaard, P., 2017. Estimation of incident and reflected components in highly nonlinear regular waves. *Coast. Eng.* 119, 51–64.
- Bredmose, H., Bullock, G., Hogg, A., 2015. Violent breaking wave impacts. part 3: effects of scale and aeration. *J. Fluid Mech.* 765, 82–113.
- Bredmose, H., Peregrine, D., Bullock, G., 2009. Violent breaking wave impacts. part 2: modelling the effect of air. *J. Fluid Mech.* 641, 389–430.
- Bullock, G., Obhrai, C., Peregrine, D., Bredmose, H., 2007. Violent breaking wave impacts. part 1: Results from large-scale regular wave tests on vertical and sloping walls. *Coast. Eng.* 54, 602–617.
- Cao, D., Yuan, J., Chen, H., Zhao, K., Liu, P.L.F., 2021. Wave overtopping flow striking a human body on the crest of an impermeable sloped seawall. part i: Physical modeling. *Coast. Eng.* 167, 103891.
- Castellino, M., Romano, A., Lara, J.L., Losada, I.J., De Girolamo, P., 2021. Confined-crest impact: Forces dimensional analysis and extension of the goda's formulae to recurved parapets. *Coast. Eng.* 163, 103814.
- Castellino, M., Sammarco, P., Romano, A., Martinelli, L., Ruol, P., Franco, L., De Girolamo, P., 2018. Large impulsive forces on recurved parapets under non-breaking waves. a numerical study. *Coast. Eng.* 136, 1–15.
- Chen, X., Hofland, B., Altomare, C., Suzuki, T., Uijtewaal, W., 2015. Forces on a vertical wall on a dike crest due to overtopping flow. *Coast. Eng.* 95, 94–104.
- Chen, H., Yuan, J., Cao, D., Liu, P.L.F., 2021. Wave overtopping flow striking a human body on the crest of an impermeable sloped seawall. part ii: Numerical modelling. *Coast. Eng.* 168, 103892.
- Cooker, M., Peregrine, D., 1990. Computations of violent motion due to waves breaking against a wall. In: Proc. 22nd Intl. Conf. on Coastal Engineering. ASCE, pp. 164–176.
- Cuomo, G., Allsop, W., Bruce, T., Pearson, J., 2010a. Breaking wave loads at vertical seawalls and breakwaters. *Coast. Eng.* 57, 424–439.
- Cuomo, G., Allsop, W., Takahashi, S., 2010b. Scaling wave impact pressures on vertical walls. *Coast. Eng.* 57, 604–609.
- de Almeida, E., Hofland, B., 2020. Validation of pressure-impulse theory for standing wave impact loading on vertical hydraulic structures with short overhangs. *Coast. Eng.* 159, 103702.
- De Finis, S., Romano, A., Bellotti, G., 2020. Numerical and laboratory analysis of post-overtopping wave impacts on a storm wall for a dike-promenade structure. *Coast. Eng.* 155, 103598.
- De Rouck, J., Van Doorslaer, K., Versluys, T., Ramachandran, K., Schimmels, S., Kudella, M., Trouw, K., 2012. Full scale impact tests of an overtopping bore on a vertical wall in the large wave flume (gwk) in hannover. *Coast. Eng. Proc.* 1 (33).
- EurOtop, 2007. Wave overtopping of sea defences and related structures: assessment manual. Pullen, T and Allsop, NWH and Bruce, T and Kortenhaus, A and Schüttrumpf, H and Van der Meer, JW.
- Goda, Y., 2010. Random Seas and Design of Maritime Structures. Volume 33. World Scientific Publishing Company.
- Kisacik, D., Troch, P., Van Bogaert, P., 2012. Description of loading conditions due to violent wave impacts on a vertical structure with an overhanging horizontal cantilever slab. *Coast. Eng.* 60, 201–226.
- Kisacik, D., Troch, P., Van Bogaert, P., Caspele, R., 2014. Investigation of uplift impact forces on a vertical wall with an overhanging horizontal cantilever slab. *Coast. Eng.* 90, 12–22.
- Kortenhaus, A., Haupt, R., Oumrari, H., 2002. Design aspects of vertical walls with steep foreland slopes. In: Breakwaters, Coastal Structures and Coastlines: Proceedings of the International Conference Organized by the Institution of Civil Engineers and Held in London, UK on 26-28 2001. Thomas Telford Publishing, pp. 220–232.
- Kortenhaus, A., Pearson, J., Bruce, T., Allsop, N., Van der Meer, J., 2004. Influence of parapets and recurves on wave overtopping and wave loading of complex vertical walls. In: Coastal Structures 2003. pp. 369–381.
- Martin, F.L., Losada, M.A., Medina, R., 1999. Wave loads on rubble mound breakwater crown walls. *Coast. Eng.* 37, 149–174.
- Martinelli, L., Lamberti, A., 2011. Dynamic response of caisson breakwaters: suggestions for the equivalent static analysis of a single caisson in the array. *Coast. Eng. J.* 53, 1–20.
- Martinelli, L., Ruol, P., Volpato, M., Favaretto, C., Castellino, M., De Girolamo, P., Franco, L., Romano, A., Sammarco, P., 2018. Experimental investigation on non-breaking wave forces and overtopping at the recurved parapets of vertical breakwaters. *Coast. Eng.* 141, 52–67.
- Molines, J., Bayon, A., Gómez-Martín, M.E., Medina, J.R., 2019. Influence of parapets on wave overtopping on mound breakwaters with crown walls. *Sustainability* 11 (7109).

- Oumeraci, H., Kortenhaus, A., Allsop, W., de Groot, M., Crouch, R., Vrijling, H., Voortman, H., 2001. Probabilistic Design Tools for Vertical Breakwaters. CRC Press.
- Pearson, J., Bruce, E.T., Allsop, W., Kortenhaus, A., van der Meer, J., 2005. Effectiveness of recurve walls in reducing wave overtopping on seawalls and breakwaters. In: Coastal Engineering 2004: (in 4 Volumes). World Scientific, pp. 4404–4416.
- Ravindar, R., Sriram, V., Schimmels, S., Stagonas, D., 2021. Approaches in scaling small-scale experiments on the breaking wave interactions with a vertical wall attached with recurved parapets. *J. Waterw. Port Coast. Ocean Eng.* 147, 04021034.
- Romano, A., Bellotti, G., Briganti, R., Franco, L., 2015. Uncertainties in the physical modelling of the wave overtopping over a rubble mound breakwater: The role of the seeding number and of the test duration. *Coast. Eng.* 103, 15–21.
- Stagonas, D., Lara, J.L., Losada, I.J., Higuera, P., Jaime, F.F., Muller, G., 2014. Large scale measurements of wave loads and mapping of impact pressure distribution at the underside of wave recurves. In: Proceedings of the HYDRALAB IV Joint User Meeting.
- Takahashi, S., 1996. Design of vertical breakwaters. breakwater design. In: International Conference on Coastal Engineering. Short Course, Orlando.
- Van Doorslaer, K., Romano, A., De Rouck, J., Kortenhaus, A., 2017. Impacts on a storm wall caused by non-breaking waves overtopping a smooth dike slope. *Coast. Eng.* 120, 93–111.
- van Gent, M.R., 2003. Wave overtopping events at dikes. In: Coastal Engineering 2002: Solving Coastal Conundrums. World Scientific, pp. 2203–2215.
- Williams, H.E., Briganti, R., Romano, A., Dodd, N., 2019. Experimental analysis of wave overtopping: A new small scale laboratory dataset for the assessment of uncertainty for smooth sloped and vertical coastal structures. *J. Marine Sci. Eng.* 7 (217).